Final Technical Report

TNW2009-02

Research Project Agreement No. 430846

Incorporation of Forward-Directivity into Seismic Hazard Analysis

Prof. Adrian Rodriguez-Marek Prof. William Cofer

Department of Civil and Environmental Engineering
Washington State University
Pullman, WA 99164

A report prepared for

Transportation Northwest (TransNow)
University of Washington
135 More Hall, Box 352700
Seattle, Washington 98195-2700

January 2009

TECHNICAL REPORT STANDARD TITLE PAGE

1. REPORT NO.	2. GOVERNMENT ACCESSION NO.	3. RECIPIENT'S CATALOG NO.
TNW2009-02		

4. TITLE AND SUBTITLE	5.REPORT DATE
Incorporation of Forward-Directivity into Seismic Hazard Analysis	January 2009
	6. PERFORMING ORGANIZATION CODE

7. AUTHOR(S)	8. PERFORMING ORGANIZATION REPORT NO.
Adrian Rodriguez-Marek, William Cofer	TNW2009-02

9. PERFORMING ORGANIZATION NAME AND ADDRESS	10. WORK UNIT NO.
Transportation Northwest Regional Center X (TransNow) Box 352700, 129 More Hall University of Washington Seattle, WA 98195-2700	11. CONTRACT OR GRANT NO. DTRS99-G-0010

12. SPONSORING AGENCY NAME AND ADDRESS	13. TYPE OF REPORT AND PERIOD COVERED
Washington State University CEE Department Pullman, WA 99164	Final Research Report
	14. SPONSORING AGENCY CODE

15. SUPPLEMENTARY NOTES

ABSTRACT

Ground motions in close proximity to the causative fault of an earthquake can be significantly affected by the propagation of rupture. In particular, when the rupture and slip direction relative to a site coincide and a significant portion of the fault ruptures towards the site, the ground motion can exhibit the effects of Forward-Directivity (FD). Forward-directivity effects can result in higher seismic demands and must be considered for design or retrofit of a structure that is in the proximity of an active fault. Much research has been conducted recently on the seismological aspects leading to forward-directivity, the characteristics of FD motions. However, designers still lack specific guidelines as to how to account for FD effects when determining the seismic hazard for a given structure.

The overall purpose of this research project is to develop a methodology for the inclusion of the effects of near-fault forward-directivity into the determination of seismic demand for a structure or a geotechnical system. The focus of the study will be the potential for near-fault effects associated with the Seattle and Tacoma faults in Washington State, and how these near-fault effects can affect the transportation infrastructure in the state.

17. KEY WORDS	18. DISTRIBUTION STATEMENT

19. SECURITY CLASSIF. (of this report)	20. SECURITY CLASSIF. (of this page)	21. NO. OF PAGES	22. PRICE
None	None	51	

DISCLAIMER

The contents of this report reflect the views of the authors, who are responsible for the facts and the accuracy of the information presented herein. This document disseminated through the Transportation Northwest (TransNow) Regional University Transportation Center under the sponsorship of the Department of Transportation University Transportation Centers Program, in the interest of information exchange. The U.S. Government assumes no liability for the contents or use thereof.

Introduction

Ground motions in close proximity to the causative fault of an earthquake can be significantly affected by the propagation of rupture. In particular, when the rupture and slip direction relative to a site coincide and a significant portion of the fault ruptures towards the site, the ground motion can exhibit the effects of Forward-Directivity (FD) (Somerville et al. 1997). FD ground motions are distinctly different from ordinary ground motions. FD ground motions are short in duration and consist of one or more pulses of motions. These pulses can result in higher seismic demands and must be considered for design or retrofit of a structure that is in the proximity of an active fault.

Modern seismic design philosophy is based in the concept of Performance Based Design (PBD), whereas the design of a structure is directed towards meeting selected target behavior levels (e.g. "Fully Operational" to "Near Collapsed") within established risk levels. These objectives are usually achieved by characterizing structural behavior in terms of a deformation measure that has a good correlation with the damage measures targeted by PBD. Within this design philosophy, seismic hazard is usually quantified through Probabilistic Seismic Hazard Analysis (PSHA), and the resulting hazard is convolved with a structural response function in what is commonly known as Probabilistic Seismic Demand Analysis (PSDA) to obtain performance measures associated with quantified risk levels. PSDA methodologies have been studied extensively for ordinary ground motions; however, the current understanding regarding FD ground motions has yet to be integrated into PSDA.

This report presents the results of research performed at Washington State University over the last two years towards the goal of developing a methodology for the inclusion of the effects of near-fault forward-directivity into the determination of seismic demand of a structure. The report first presents a technical background on the characteristics of forward directivity ground motions and the implementation of performance based design. The methodology developed for time-domain PSDA of forward directivity ground motions is then presented. Finally, the results of the proposed PSDA methodology are applied on a sample MDOF system to exemplify the importance of considering forward-directivity ground motions in design.

Background

Forward-Directivity

In the near-fault region, ground motions at a particular site are significantly influenced by the rupture mechanism and the rupture direction relative to the site, as well as the permanent ground displacement at the site resulting from tectonic movement. Depending on the first two factors, ground motions in the near-fault zone can exhibit the dynamic consequences of “forward-directivity,” “neutral-directivity,” or “backward-directivity.” Depending on the last factor, ground motions close to the rupture surface may contain a significant permanent static displacement, which is termed “fling-step” (Bray and Rodriguez-Marek 2004). The estimation of ground motions for a project site close to an active fault should account for these special aspects of near-fault ground motions. The "fling-step" usually induces only limited inertial demands on structures due to the long-period nature of the static displacement. On the other hand, ground motions that are influenced by forward-directivity effects can be very damaging to structures. Forward-directivity effects are seen when the rupture direction is aligned with the direction of slip, and the rupture front moves towards a given site (Bray and Rodriguez-Marek 2004). These conditions occur readily in strike-slip earthquakes when the rupture propagates horizontally towards a given site. Forward-directivity conditions are also met for dip-slip faulting at sites that are located close to the surface projection of the fault. Note that two of the larger urban centers of Washington State, Seattle and Tacoma, are traversed by faults that can potentially generate forward-directivity effects. This implies that a large inventory of civil and transportation infrastructure (e.g., bridges, retaining walls, port facilities) are vulnerable to forward-directivity ground motions (FDGMs).

Forward-directivity ground motions typically contain very few long period, high intensity ground motion pulses that are best observed in velocity time histories. Due to the radiation pattern of the fault, these pulses are typically aligned with the fault normal direction. However, strong pulses may be present in the fault parallel direction as well (Bray and Rodriguez-Marek 2004). These motions typically have a short duration with amplitudes larger than those of generic motions, and with a strong preferential fault-normal orientation. The differences between FDGMs and "ordinary" ground motions recorded away from the fault can be summed up as:

a) The velocity-time histories of FDGMs consist of a few (two to six) long-period pulses.
b) FDGMs have higher spectral accelerations in a period band centered on the period of the forward-directivity pulse. This period ranges from 0.6 s to upwards of 5 s (Bray and Rodriguez-Marek 2004).
c) FDGMs have larger peak ground velocities (PGV), in particular in the fault-normal direction.
d) FDGMs have shorter durations.

With the exception of item (d), all other particularities of FDGMs imply that they will produce higher demands on structures or geotechnical systems. Currently there are two approaches used to deal with forward directivity effects. In the *spectral* approach, rupture directivity effects are generally taken into account by modifications to the elastic acceleration response spectrum at 5% damping (Somerville et al. 1997, Somerville 2003, Spudich and Chiou 2008). This approach lends itself readily to inclusion into Probabilistic Seismic Hazard Analyses (e.g., see Abrahamson 2000). In the *time-domain* approach, FD effects are characterized by parameters obtained from time domain representations of the ground motion (e.g. pulse period and pulse amplitude, see Mavroeidis and Papageorgiou 2003, Bray and Rodriguez-Marek 2004, Baker 2007). This is because traditional response spectrum representations of ground motions do not adequately represent the demand for a high rate of energy absorption presented by near-fault pulses. More specifically, when the high intensity levels of these motions drive structures into the nonlinear range, the linear-elastic assumption underlying the response spectrum concept is invalidated (Somerville 2003). There is considerable argument over which one of these approaches is correct. For example, Malhotra (1999) and Chopra and Chintanapakdee (2001) indicate that modifications to the linear and nonlinear design spectra are enough to capture structural response to FDGMs. On the other hand, other researchers have indicated that time-domain analyses are better suited for pulse-type motions and that structural performance is significantly influenced by the characteristics of the velocity-time history (e.g. Anderson and Bertero 1987, Hall et al. 1995, Makris 1997, Alavi and Krawinkler 2000, Sasani and Bertero 2000, Mylonakis and Reinhorn 2001, and Zhang and Iwan 2002). Our research indicates that taken as a group, forward-directivity ground motions are more damaging for the same level of

spectral accelerations than non-forward directivity ground motions. There is, however, no argument in the fact that FD effects must be considered in design of structures and geotechnical systems; and that time-history analysis for nonlinear structures is necessary even if it is only as a design check.

Although FDGMs pose a significant threat to structures, this threat is not equal for all structures. For example, coincidence of the structure and pulse period leads to amplification of structural response. However, the period of the structure and the pulse period can vary significantly. The FDGM pulse period is proportional to the earthquake magnitude, lengthening as the earthquake magnitude increases. As a result, damage due to smaller magnitude earthquakes can be more significant for short period structures than damage due to larger magnitude earthquakes, since the near-fault pulse period is closer to the fundamental period of the structure in the smaller magnitude earthquake. This contradicts conventional engineering intuition that directly correlates damage potential with earthquake magnitude, thus highlighting the need for a unique way to accurately assess the potential for structural damage due to FDGMs. The near-fault pulse can impose an additional damage variable on structures: large residual deformations. Although consisting only of a few cycles, the pulses can impose large inelastic drift on structures, resulting in significant permanent deformations. Not only are conventional damage indices such as maximum displacement and energy absorbed important for assessing the response of structures, alternatives including residual displacement are necessary as well (Priestley, 2003).

Performance Based Earthquake Engineering

The second generation of Performance-Based Earthquake Engineering assessment and design procedures (PBEE-2) are postulated based on probability-based performance assessment tools (Cornell et al. 2002). PBEE-2 is expressed in terms of a triple integral:

$$\lambda(DV) = \iiint P[DV \mid DM]dP[DM \mid EDP]dP[EDP \mid IM]\,|\,d\lambda[IM]\,| \qquad (1)$$

where DV, DM, EDP, and IM are decision variable, damage measure, Engineering Demand Parameters, and Intensity Measure, respectively. P[X|Y] is the probability density of X conditioned on knowledge of Y, and $d\lambda[IM]$ is mean annual frequency of occurrence of the IM.

Probabilistic evaluation of EDPs in terms of Intensity Measures is known as Probabilistic Seismic Demand Analysis and is a prerequisite for the solution of Equation 1. PSDA is built upon the more traditional PSHA and couples the probabilistic description of future ground motions from PSHA, with their random dynamic effects on a structure. Results of PSDA provide the annual likelihood of different Performance Levels for given hazard (e.g. by defining performance in terms of structural response). PSDA is embodied in the following equation (ATC-58 2004):

$$\lambda_{EDP}(x) = \int P[EDP \geq x \mid IM = y] \mid d\lambda_{IM}(y) \mid \tag{2}$$

Where $\lambda_{EDP}(x)$ is the mean annual frequency of EDP exceeding the value x, $P[EDP \geq x|IM = y]$ is the probability of EDP exceeding x given that IM equals y, $d\lambda_{IM}(y)$ is the mean annual frequency of occurrence of IM equal to y, and $\lambda_{IM}(y)$ is mean annual frequency of exceedance of the IM (e.g., the ground motion hazard) which is obtained from conventional PSHA.

In traditional PSDA analyses, the structural response, as expressed in the equation $P[EDP \geq x|IM = y]$, is obtained from a regression analyses on structural response to a series of pre-selected ground motion time histories. This approach has been extensively discussed by Baker (2007). An alternative method of design is to perform PSHA analyses to quantify the ground motion hazard and then perform time domain analyses for selected ground motions using criteria based on the equal hazard spectra along with deaggregation results. Yet another alternative arises for ground motions that are characterized by simple time histories, such as FDGM. In these cases, it is possible to perform time domain analyses within the PBD integral shown in Equation 2. This alternative approach is developed in this work.

Problem Statement

The previous discussion highlights knowledge of FDGMs. Despite this thorough understanding of the phenomena, designers are still unclear as to how the effects of FDGMs must be included into the prediction of seismic hazard. Abrahamson (2000) has shown how to incorporate forward directivity into PSHA for the determination of *elastic response spectra*. A similar methodology *does not exist* when these motions are characterized in the time domain. Moreover, there are no guidelines for the selection of time histories for design when time

histories are not fully characterized by the elastic response spectra (e.g., FDGMs). Time-history analyses are necessary for the analysis of non-linear systems subject to strong ground motion (e.g. structures taken to large loads or the response of a liquefiable soil to seismic ground motion).

Research Objectives

The goal of this study is to obtain explicit estimates of seismic demand for structures subjected to near-fault through a methodology that permits time-domain Probabilistic Seismic Demand Analysis. Probabilistic methods are utilized to include the effects of pulse-like ground motions on Intensity Measures and Engineering Demand Parameters. The novelty of the proposed approach lies on the use of equivalent pulses and time-domain analyses within the PSDA methodology. The outcome of the proposed methodology is a seismic hazard curve for an arbitrary EDP that includes the effects of forward-directivity. This overall goal can be divided into the following objectives:

a) Develop an equivalent pulse model to represent the characteristics of pulse-like ground motions based on an empirical analysis of the ground motion database.
b) Utilize the equivalent pulse model to evaluate EDPs through Incremental Dynamic Analysis (IDA) for near-fault ground motions with dominant forward-directivity pulse.
c) Incorporate the use of equivalent pulses into Probabilistic Seismic Demand Analysis for the selected EDPs.
d) Demonstrate the applicability of the proposed methodology on a selected structure and quantify the difference in hazard estimates resulting from the use of the proposed methodology as compared with state-of-the-art methods.

Method of Analysis

The proposed methodology is developed herein. In order to better present the methodology, a structure is first selected such that the proposed methodology can be explained with a tangible example. A more extensive development of the proposed methodology is presented in the Ph.D. thesis of Sehhati (2008). The development herein is simplified for clarity of presentation, yet an attempt to make it self-sufficient is also made.

Selection of a structural system and structural analysis methodology

For simplicity and in order to maintain a non-specific approach, a generic building was considered in the development of the model. The building is a seven-story building designed as regular structure, both in plant and in height, with fundamental period of exactly 1.0 second. The structure was designed to have a base shear coefficient (defined as the base shear that causes yielding in the structure divided by the total weight of the structure) of 0.07. The seismic resisting system in the weak direction consists of four moment resisting steel frames. Each frame has three 20 feet long by 12.5 feet high spans. Details of the building in the strong direction are irrelevant in this study because the structures were only loaded in their weak direction. To reduce computational efforts, the structures were simplified by shear building models.

A MATLAB program was written for conducting 2D nonlinear dynamic analyses of the frames. The step-by-step integration method with the Wilson-Theta modification (Chopra 1995) was used for time integration and the Modified Newton-Raphson Method (Chopra 1995) was used to iterate within each time step. Steel material nonlinearity was modeled by an elastoplastic kinematic hardening relationship, having identical properties in tension and compression. The frames were assumed to have a viscous damping ratio equal to 5%. To enhance analysis accuracy, each story was modeled in SAP2000 and subjected to pushover analysis to get a force-displacement curve for that story. Plastic hinge properties of each member were modeled with a bilinear non-degrading moment-curvature model with a range of strain hardening from 2.5% to 3.5%. These models were obtained from the commercial Xtract software and were assigned to the SAP model at top and bottom of columns. The member hardening behavior in each story resulted in a story hardening stiffness range of 10% to 12% in form of force-displacement curves. The force-displacement curves obtained from SAP pushover analyses for each story were used by the MATLAB program for the dynamic analyses.

P-Δ effects, which can have a significant role in the response of near-fault structures with an excessive drift, were approximated by adding geometric stiffness to the first order stiffness matrix (see Sehhati 2008 for details). The geometric stiffness was formed assuming that axial forces remain constant for the entire duration of the ground motion. Geometric stiffness was calculated based on the shape functions of each column with the two ends fixed against rotation and found to be equal to 1.2P/L where P is axial load and L is length of column.

Engineering Demand Parameters such as drift ratio, ductility demand, and story shear forces were monitored. However, the maximum story displacement ductility demand (MSDD) was selected to describe the inelastic response of the structures. The MSDD becomes greater than 1.0 when the relative displacement in any story is larger than the story yield displacement. The maximum inter-story ductility demand (MIDD) was defined as the maximum value of the MSDD over all the stories and is used heretofore as the EDP to characterize structural response.

Statistical Models to Correlate EDPs to IMs

The building described above was subject to ground motions recorded within 20 km from a fault (see Sehhati 2008 for details on the ground motions used). The near-fault ground motions were divided in two groups, one group consisting of ground motions with pulses as identified by the procedure of Baker (2007), and the other group for ground motions without pulses. A power-law relationship between MIDD and $Sa(T_1)$ was assumed. The parameters of the relationship were obtained using a Maximum Likelihood regression assuming a normal distribution for MIDD. For near-fault motions without pulses the resulting relationship is given by:

$$\overline{MIDD} = \begin{cases} 1 + 13(S_a(T_1) - 0.1)^{0.7} & for\ Sa > 0.1 \\ 1 & for\ Sa \le 0.1 \end{cases} \tag{3a}$$

with σ given by

$$\sigma = \begin{cases} \sigma_{\min} & for\ S_a \le x_o \\ (\sigma_{\max} - \sigma_{\min})\dfrac{S_a - x_o}{x_1 - x_o} + \sigma_{\min} & for\ x_1 > S_a > x_o \\ \sigma_{\max} & for\ S_a \ge x_1 \end{cases} \tag{3b}$$

where $x_o = 0.1$, $x_1 = 0.57$, $\sigma_{\max} = 1.98$, and $\sigma_{min} = 0.34$. The range of applicability of Equation 3a is $0 < S_a(T_1) \le 1.9$g. It was assume that MIDD has a normal distribution with mean given by Equation 3a and standard deviation given by Equation 3b. However, the normal distribution is truncated to prevent physically unrealizable MIDD values (e.g. MIDD<1). Alternative distributions to the normal distribution were attempted but they all resulted in poor fits to the

residuals for high values of MIDD. Similarly, another power relationship between $S_a(T_1)$ and *MIDD* for the near-fault ground motion with pulses dataset was computed:

$$MIDD = 1 + 24.6(S_a(T_1) - 0.1)^{0.71} \tag{4}$$

with σ given by Equation 3b with $x_o = 0.1$, $x_1 = 1.24$, $\sigma_{\max} = 8.54$, and $\sigma_{min} = 2.11$. The applicability range for Equation 4 is $0 < S_a(T_1) \leq 1.9$g. As for non-pulse ground motions, it was assume that MIDD has a normal distribution with the mean value given by Equation 4 and the standard deviation given by Equation 3b with the parameters indicated above. Figure 1 compares predicted EDPs from Equation 3 and 4 with EDPs computed for each of the ground motions in the data set. Observe the clear difference in behavior for pulse-like and non-pulse-like ground motions. Pulse like ground motions elicit a higher structural response for the same level of spectral acceleration. Moreover, the spread for pulse-like ground motions is higher (e.g. higher standard deviation) than for non-pulse-like ground motions, indicating that $Sa(T_1)$ is not a good predictor of structural response for pulse-like ground motions.

Development of an equivalent pulse model for forward-directivity ground motions

Wavelets are basis functions that can be used to divide a given function or continuous-time signal into different frequency components. Mavroeidis and Papageorgiou (2003) modified the Gabor (1946) wavelet by replacing the Gaussian envelope of the Gabor wavelet with another symmetric bell-shaped function that possesses a simpler analytical expression. The velocity time history of the resulting wavelet is expressed as:

$$V(t) = \begin{cases} A\frac{1}{2}[1+\cos(\frac{2\pi f_p}{\gamma}(t-t_0))]\cos[2\pi f_p(t-t_0)+\nu], & t_0 - \frac{\gamma}{2f_p} \leq t \leq t_0 + \frac{\gamma}{2f_p} \quad with \ \gamma > 1 \\ 0, \ otherwise \end{cases} \tag{5}$$

where, A controls the amplitude of the wavelet, f_p is the frequency of the amplitude-modulated harmonic (or the prevailing frequency of the signal), ν is the phase of the amplitude-modulated harmonic (i.e., $\nu = 0$ and $\nu = \pm\pi/2$ define symmetric and antisymmetric signals, respectively), γ is a parameter that defines the oscillatory character (i.e., zero crossings) of the signal, and t_o

specifies the location in time of the envelope's peak. An illustrative example of this pulse is shown in Figure 2. In this study, only $\nu = 0$ was considered in order to achieve an equivalent pulse with a lower number of parameters. Hence, the parameters needed to define the Gabor wavelet pulse are A, f_p, and γ.

A set of recorded forward directivity ground motions was assembled and is presented in detail in Sehhati (2008, see also the Appendix). Each of these pulse-like ground motions was associated with a pulse period (using the procedures of Baker 2007 and Bray and Rodriguez-Marek 2004) and the amplitude of the dominant pulse. For each recorded FD ground motion, non linear structural analyses were conducted and the response in terms of MIDD was compared to the structural response obtained using the simplified pulses as input motions. The results can be summarized as follows:

- If the pulse period is in the neighborhood of the structural period, then the response of the structure is controlled by the forward directivity pulse and, more significantly, the simplified pulse representations using the pulse parameters obtained directly from the ground motions render similar structural response to the recorded ground motions. For the particular structure in consideration, it was determined that the pulse controls response when 0.5 s $\leq$ Tp/Ts $\leq$ 2.5, where T_p and T_s are the pulse period and the structural period, respectively.
- The pulse amplitude of the Gabor pulses that best mimics structural response is on average 73% of the peak ground velocity.

The relationship between pulse period and magnitude is obtained from Baker (2007):

$$Ln(\overline{T}_p) = -5.78 + 1.02 M_w \text{ with } \qquad \sigma_{\ln T_p} = 0.55 \tag{6}$$

where $\overline{T}_p$ is the median predicted value of pulse period in seconds as a function of magnitude, M_w; and $\sigma_{\ln T_p}$ is the standard deviation in natural log units of the pulse period. This Equation implicitly assumes that the pulse period has a log normal distribution. Similar relationships were proposed by Bray and Rodriguez-Marek (2004) and Mavroeidis and Papageorgiou (2003), among others.

The pulse amplitude A_p can be calculated using predictive relationships for PGV. The model of Bray and Rodriguez-Marek (2004) is used to estimate PGV at distances shorter than 20 km (the limit of applicability of that model):

$$Ln(\overline{PGV}) = 4.51 + 0.34M_w - 0.57Ln({r_{rup}}^2 + 7^2) \quad \text{with} \qquad \sigma_{PGV} = 0.49 \tag{7}$$

where $\overline{PGV}$ is in units of cm/sec, r_{rup} is the closest distance to the site in km, and σ_{PGV} is the standard deviation of PGV in log units. It is assumed that PGV is lognormally distributed. At distances larger than 60 km, the PGV is estimated using the Abrahamson and Silva NGA relationship (2007). For intermediate distances (e.g. between 20 km and 60 km), a cosine taper function is used to transit smoothly from the near-source PGV correlation (Bray and Rodriguez-Marek 2004) to the NGA PGV correlation (Abrahamson and Silva 2007):

$$Ln(\overline{PGV}) = \phi.Ln(\overline{PGV}_{Rodriguez-Marek}) + (1-\phi).Ln(\overline{PGV}_{NGA}) \tag{8}$$

where $\phi = \frac{1}{2} + \frac{1}{2}\cos(\pi(\frac{r_{rup}}{40} - \frac{1}{2}))$. Figure 3 shows an example of the resulting PGV function. The standard deviation of PGV is similarly defined. The pulse period and pulse amplitude were determined to be positively correlated, but their residual values are uncorrelated hence the two variables can be treated as statistically independent random variables.

Incremental Dynamic Analyses for simplified pulses

Given that Gabor wavelet pulses can reasonably represent near-fault ground motions when their pulse period is in the neighborhood of the fundamental period of the structure ($0.5 \leq T_{pulse}/T_{structure} \leq 2.5$ for the structures studied herein), multiple runs can be used to predict the inelastic response of the structure for pulses with all possible amplitudes and periods in this range; thus the inelastic response of structures can be predicted for a range of forward-directivity pulses with realistic amplitudes and frequencies (Figure 4). The short period region of the response surface in Figure 4 is less smooth than the response at other period ranges, indicating that there are no clearly defined trends in the response of the structure in this region. This likely happens because the contribution of higher modes becomes predominant.

Proposed PSDA methodology: A Time-Domain PSDA methodology

Similar to the procedure set forth by Tothong et al. (2007), the proposed methodology separates the mean annual frequency of exceedance (MAF) of an Engineering Demand Parameter for a given Intensity Measure, $\lambda_{EDP}(x)$, into two parts; near-source (NS) and non-near-source (non-NS). This is expressed as:

$$\lambda_{EDP}(x) = \lambda_{EDP,non-NS}(x) + \lambda_{EDP,NS}(x) \tag{9}$$

The MAF of the EDP for the near-source case ($\lambda_{EDP,NS}$) includes hazard resulting from pulse- and non-pulse-like ground motions and can be separated into two parts: the near-source hazard from pulse-like ground motion events, $\lambda_{EDP,NS\&pulse}$, and the near-source hazard due to non–pulse-like records, $\lambda_{EDP,NS\&no-pulse}$:

$$\lambda_{EDP,NS}(x) = \lambda_{EDP,NS\&pulse}(x) + \lambda_{EDP,NS\&no-pulse}(x) \tag{10}$$

For near-source ground motion with forward-directivity pulses, two different cases are considered:

1. When forward-directivity pulses are not dominant: in this case, forward-directivity pulses do not control response of the structure, hence, $S_a(T_1)$ is used as an Intensity Measure. These cases are treated similarly to near-source events without pulse.
2. When forward-directivity pulses are dominant: in this case, forward-directivity pulses control structural response and simplified pulses are used to predict the EDP using time-domain analyses.

For the MDOF structure used as an example herein, when the ratio of the pulse period and structural period are within 0.5 and 2.5 (e.g., $0.5 \leq T_{pulse}/T_{structure} \leq 2.5$), forward-directivity pulses are dominant and control the behavior of the structures. For these cases, Figure 4 can be sued to predict the EDP for possible forward-directivity pulses. Note that the bounds for which the pulse controls ($T_{lower} = 0.5\ T_p$ and $T_{upper} = 2.5\ T_p$ for the MDOFs studied herein) may be structure dependent. Nonetheless, the concept that the response of the structure is controlled by

the pulse when the pulse period is in the neighborhood of the structural period is assumed to be generally applicable to all structures.

In summary, the EDP hazard at a site can be divided into

$$\lambda_{EDP}(x) = \lambda_{EDP,non-NS}(x) + \lambda_{EDP,NS\&no-pulse}(x) + \lambda_{EDP,NS\&pulse,\text{pulse is dominant}}(x) + \lambda_{EDP,NS\&pulse,\text{pulse is not dominant}}(x) \quad (11)$$

For non-near source ($\lambda_{EDP,non-NS}$), and near source cases with no pulse or in which the pulse is not dominant ($\lambda_{EDP,\ NS\&no-pulse}$ and $\lambda_{EDP,NS\&pulse,\ pulse\ is\ not\ dominant}$), λ_{EDP} is computed from Equation 2, hence statistical correlations between the EDP (MIDD) and the IM (spectral acceleration) are used (e.g. Equations 3 and 4). In these cases, the intensity measure hazard (λ_{Sa}) has to be deaggregated into the same four scenarios considered for the EDP, hence:

$$\lambda_{S_a}(x) = \lambda_{S_a,non-NS}(x) + \lambda_{S_a,NS\&no-pulse}(x) + \lambda_{S_a,NS\&pulse,\text{pulse is dominant}}(x) + \lambda_{S_a,NS\&pulse,\text{pulse is not dominant}}(x) \quad (12)$$

Each of these hazard components is discussed in the following subsections.

Hazard for non-near source scenarios [$\lambda_{EDP,non-NS}(x)$]

Whenever the closest distance to the ruptured fault for a given scenario is greater than 60 km, that scenario is considered to be a non-near source scenario. The 60 km threshold distance is based on Abrahamson's (2000) model. For these cases, the mean annual frequency of the Engineering Demand Parameter exceeding x (for a given IM, which for this case is $S_a(T_1)$) for non-near-source events, $\lambda_{EDP,Non-NS}(x)$, is given by:

$$\lambda_{EDP,Non-NS}(x) = \int P[(EDP \geq x) \mid S_a = y] \mid d\lambda_{S_a,Non-NS}(y) \mid \quad (13)$$

where $P[(EDP \geq x) \mid S_a = y]$ is the conditional probability of EDP exceeding x given that $S_a(T_1) = y$. In this step, EDP and IM are correlated through Equation 3. $d\lambda_{S_a}(y)$ is the mean annual frequency of occurrence of $S_a(T_1) = y$. $d\lambda_{S_a}(y)$ is equal to $\lambda_{S_a}(y - \Delta/2) - \lambda_{S_a}(y + \Delta/2)$,

where Δ is a selected Intensity Measure interval and $\lambda_{S_a,Non-NS}(y)$ is the mean annual frequency of elastic-pseudo spectral acceleration exceeding *y* and is obtained through conventional PSHA. For non-near-source ground motion events (e.g. for distances greater than 60 km) $\lambda_{S_a,Non-NS}(y)$ is given by:

$$\lambda_{Sa,Non-NS}(y) = \sum_{i=1}^{\#faults} \nu_i \iint_{m_w,r_{rup}} \left[1 - I_{NS}\left(r_{rup}^i\right)\right] G_{Sa|M_w^i,R_{rup}^i}\left(y \mid m_w, r_{rup}\right) \cdot f_{M_w^i,R_{rup}^i}\left(m_w, r_{rup}\right) dm_w . dr_{rup} \tag{14}$$

where v_i is the mean annual rate of occurrence of earthquakes on fault *i* above a minimum threshold magnitude, M_w is the moment magnitude, and R_{rup} is the closest distance from the site to the rupture plane. The function $I_{NS}(r_{rup})$ is a flag that is set to one when $r_{rup} < 60$ km, and set to 0 when $r_{rup} > 60$ km. The term $f_{M^i,R_{rup}^i}(m_w, r_{rup})$ is the joint probability density function (PDF) of M_w and R_{rup} on fault *i*. The term, $G_{Sa|M_w^i,R_{rup}^i}(y \mid m_w, r_{rup})$, represents the Complementary Cumulative Gaussian probability density function (CCDF) of the log normally distributed random variable S_a, which is defined as:

$$G_{Sa|M_w^i,R_{rup}^i}(y \mid m_w, r_{rup}) = 1 - \Phi\left(\frac{\ln y - \mu_{\ln S_a|m_w,r_{rup}}}{\sigma_{\ln S_a|m_w,r_{rup}}}\right) \tag{15}$$

where $\Phi(...)$ is the standard Gaussian CDF, and $\mu_{\ln S_a|m_w,r_{rup}}$ and $\sigma_{\ln S_a|m_w,r_{rup}}$ are the conditional mean and standard deviation of the natural logarithm of S_a, respectively, as obtained from a ground motion prediction model (e.g. Abrahamson and Silva 2007), and *y* is a test value for S_a. Note that in random variables are denoted by uppercase characters while lowercase characters represent realizations of those random variables. Equation 14 sums the hazard over all faults affecting a site. Without loss of generality, the presentation from here on assumes that a single fault contributes to hazard and the subscript *i* is ignored.

A note on the implementation of Equation 14 is in order here. The definition of the joint probability density function $f_{M,R_{rup}}(m_w, r_{rup})$ requires the definition of the probability density

function for closest distance to the fault (R_{rup}) which in turn is a function of magnitude through the dependence of rupture length on magnitude. An alternative approach is to iterate through all possible scenarios for magnitude and rupture length in which case Equation 14 becomes (for a single fault):

$$\lambda_{Sa,Non-NS}(y) = \upsilon \int_{m_w} \int_{rl} \int_{\chi} \left[1 - I_{NS}(r_{rup})\right] G_{Sa|M_w,R_{rup}}(y \mid m_w, r_{rup}) \cdot f_{M_w}(m_w) f_{RL}(m_w) f_{\mathrm{X}}(m_w, rl) . dm_w . drl . d\chi \quad (16)$$

where RL is the rupture length and X is the location of the ruptured segment within the given fault. Note that r_{rup} is a function of χ and rl, but the functionality is omitted from the notation of Equation 16 for simplicity. The probability density function for magnitude, $f_{Mw}(m_w)$ can be obtained by geological or seismological analyses and is usually defined for a given fault (McGuire 2004). The probability density function for rupture length, $f_{RL}(m_w)$ is given by empirical relationships such as Wells and Coppersmith (1984). The probability density function for the location of rupture (f_{X}) is assumed to be uniform, implying equal probability of occurrence of rupture within the fault. This is a simplification that may not apply for faults with strong segmentation. Equation 16 is easier to implement numerically than Equation 14 and lends itself to implementation of forward-directivity as discussed in subsequent sections.

The implementation of Equation 16 is carried through the discretization of its integrals. The predictor variables for magnitude (M_w), rupture length (RL) and location of the rupture length (X) are first discretized into bins and then Equation 4-15 can be rewritten as:

$$\lambda_{Sa,Non-NS}(y) = \upsilon \sum_{m_j} \sum_{rl_k} \sum_{\chi_m} \left[1 - I_{NS}(r_{rup})\right] G_{Sa\ |M_w,R_{rup}}(y \mid m_j, r_{rup}) P_M(m_j) P_{RL}(rl_k) P_{\mathrm{X}}(\chi_m) \quad (17)$$

where m_j, rl_k, and χ_m are the center point of the M_w, RL, and X bins, respectively; j, k, and m are summation indices; $P_M(m_j)$ denotes the probability that the magnitude falls within the j magnitude bin; $P_{RL}(rl_k)$ denotes the probability that the rupture length falls within the k rupture length bin; and $P_X(\chi_m)$ denotes the probability that the location of the rupture falls within the m_{th} bin for location of rupture. These discrete probabilities are obtained from the corresponding probability density functions in Equation 16.

Near source scenarios when no pulses are present [$\lambda_{EDP,NS\&No\text{-}Pulse}(x)$]

The approach for near-source ground motions without pulses is identical to that for non-near source ground motions, except that the IM motion hazard has to consider only the appropriate scenarios (near-source scenarios with no pulses). Whenever the closest distance to the fault was less than 60 km, that scenario was considered to be a near source scenario. The mean annual frequency of Engineering Demand Parameter exceeding x for near-source no-pulse-like events, $\lambda_{EDP,NS\&No-Pulse}(x)$, is given by Equation 2 but using $\lambda_{Sa,NS\&No\text{-}Pulse}$ as the intensity measure. The hazard curve for $\lambda_{S_{a,NS\&No-Pulse}}(y)$ and is given by:

$$\lambda_{Sa,NS\&No-Pulse}(y) = \nu \int_{m_w} \int_{rl} \int_{x} \int_{h} I_{NS}(r_{rup}) G_{Sa\,|M_w,R_{rup},No-Pulse}(y \mid m_w, r_{rup}, Z) \\ .(1 - P(pulse \mid r_{rup}, S, \theta)).f_{M_w}(m_w).f_{RL}(m_w).f_X(m_w, rl).f_H(h).dm_w.drl.dx.dh \quad (18)$$

where H is the location of the hypocenter defined between the interval [0,1] where h=0 and h=1 imply either end of the ruptured fault, and the variables Z, S, and θ are parameterizations used to characterize forward-directivity ground motions (Somerville et al. 1997). S, and θ were previously defined, and Z is defined as $\xi cos(\theta)$, where ξ is the fraction of the fault rupturing towards a site ($\xi = S/RL$). All other variables were previously defined. The probability of pulse occurrence *P(pulse)* is the probability of occurrence of a pulse and is given by Iervolino and Cornell (2008). For simplicity, in this work the location of the hypocenter is assumed to be at either end of the ruptured fault and rupture direction is then assumed to progress towards the opposite end of the fault. This implies that f_H is a discrete function that takes values of 0.5 for h=0 or h=1 (e.g. the hypocenter is located at either end of the fault). In Equation 18, r_{rup} is a function of rupture length (rl) and the location of the ruptured segment (χ). The variables S and θ are a function of the location of the hypocenter (h), the location of the fault segment (χ) and the rupture length. The term $G_{S_a|M_w,R_{rup},No-Pulse}$ is defined by Equation 15 and represents the Complementary Cumulative Gaussian distribution function of S_a conditioned on M_w, R_{rup} when no pulse-like ground motions are considered. Such an attenuation relationship could be derived by excluding pulse-like ground motion from the database. Although no such relationship has been derived to date, such a relationship could be approximated by considering the Somerville et

al. (1997) model for backward directivity. Equation 18 is solved through a discretization similar to that described by Equation 14. Such discretization is omitted herein for brevity.

Near source scenarios when Forward-Directivity pulses are not Dominant [$\lambda_{EDP,NS\&Pulse,\ pulse\ not\ dominant}(x)$]

As it was previously discussed, whenever the forward-directivity pulse is within a certain interval that contains the predominant period of the structure, then the structural response is controlled by the forward-directivity pulse. Assuming a log-normal distribution for the period of the velocity pulse, the probability that the forward-directivity pulse is within a certain range of the structural period is given by:

$$P_{within}(T_1 |\ T_p, \sigma_{Tp}) = F(ln(T_{upper}) \mid ln(T_p), \sigma_{Tp}) - F(ln(T_{lower}) \mid ln(T_p), \sigma_{Tp}) \qquad (19)$$

where T_1 is the predominant period of the structure, T_p and σ_{Tp} are the mean value and standard deviation of the pulse period which in turn are function of earthquake magnitude (Equation 6). T_{upper} and T_{lower} define the upper and lower period bounds where the structural response is controlled by the forward-directivity pulse. Such ranges were deemed to be equal to $T_{upper} = 2.5\ T_1$ and $T_{lower} = 0.5\ T_1$ for the MDOF structure analyzed herein.

The method of determining the mean annual frequency of exceedance of an EDP when forward-directivity pulses are not dominant is similar to Equation 2. The sole modification is that $S_a(T_1)$ is defined only for those near-source scenarios with pulses that are outside the pulse period range defined above. For these cases, the hazard curve is given by:

$$\begin{aligned}\lambda_{Sa,NS\&Pulse,not\ dominant}(y) = \nu \int_{m_w} \int_{rl} \int_{x} \int_{h} & I_{NS}(r_{rup}) G_{Sa|M_w,R_{rup},Pulse}(y \mid m_w, r_{rup}, Z) \\ & .(1 - P(pulse \mid r_{rup}, S, \theta)).(1 - P_{within}(T_1, M_w)).f_{M_w}(m_w).f_{RL}(m_w).f_X(m_w, rl) \\ & .f_H(h).dm_w.drl.dx.dh\end{aligned} \qquad (20)$$

Note that in this section the Complementary Cumulative Gaussian distribution function of S_a ($G_{Sa|M,Rrup,Pulse}$) should be computed from an attenuation relationship that considers pulse-like ground motions, such as the broadband directivity model of Somerville et al. (1997). Equation 21

is solved through a discretization similar to that described by Equation 14. Such discretization is omitted herein for brevity.

Near source scenarios when Forward-Directivity pulses are Dominant [$\lambda_{EDP,NS\&Pulse,pulse\ dominant}(x)$]

The treatment of near source scenarios (e.g. $r_{rup} < 60$ km) when the directivity pulses are dominant (e.g. $T_{lower} < T_p < T_{upper}$) differs from the treatment of other sources in hazard. Rather than using Equation 2 to compute the EDP risk curve, each possible scenario is considered along with the probability of occurrence of that scenario. For each scenario, the EDP is interpolated from Figure 4.

For simplicity, $\lambda_{EDP,NS\&Pulse,\ pulse\ dominant}(x)$ is defined through a discrete form of the hazard integral rather than its integral form. In schematic form, it is given as:

$$\lambda_{\mathrm{EDP,NS\&Pulsedominant}}(x) = \nu \sum_{\text{all scenarios}} \mathrm{P_{scenario}} \cdot \mathrm{I_{within}}(\mathrm{T_p}) \cdot \mathrm{I_{NS}}(r_{rup}) \cdot P_{pulse} \cdot \mathrm{H}(\mathrm{EDP_{scenario}}(\mathrm{T_p}, \mathrm{A_p}) - \mathrm{x}) \tag{21}$$

Where $I_{within}(.)$ is a flag that is equal to one when T_p falls within the interval [T_{lower}, T_{upper}] and zero otherwise, $I_{NS}(.)$ is a flag that is equal to 1 when $r_{rup} < 60$ km and zero otherwise, H is the Heaviside step function ($H(x) = 0$ for $x < 0$, and $H(x) = 1$ for $x \geq 0$), and P_{pulse} is given by Iervolino and Cornell (2008). The functions $I_{within}(.)$, and $I_{NS}(.)$ are included in the summation to eliminate all scenarios that do not qualify as near-source scenarios with pulse period in the range where the pulse period is dominant. Each scenario is weighted by the probability of that scenario taking place (discussed below), and the probability of that scenario having a pulse $P(pulse \mid r_{rup}, S, \theta)$. Finally, the function $H(.)$ ensures that only the scenarios that contribute to the hazard (e.g. where $EDP > x$) are considered for $\lambda_{EDP,NS\&Pulse,pulse\ dominant}(x)$. $EDP_{scenario}(T_p, A_p)$ is the EDP computed from time-domain analyses for a given pulse period and pulse amplitude using the Gabor pulse as the equivalent pulse representations (Figure 4)

The summation over all possible scenarios implies a multiple summation over all possible realizations of the predictive variables, namely magnitude (M_w), rupture length (RL), rupture location (X), hypocenter location (H), pulse period (Tp), and pulse amplitude (Ap). Each of these variables is discretized into bins. The probability of an individual scenario is given by:

$$P_{scenario} = P_M(m_w)\, P_{RL}(rl|m_w)\, P_X(\chi|rl)\, P_H(h)\, P_{Tp}(t_p|m_w)\, P_{Ap}(a_p|m_w,r_{rup}) \quad (22)$$

where the lower case variables represent the center point of each corresponding bin (the summation indices are omitted for clarity). The discrete probabilities P are computed using the continuous definitions given earlier. Note that pulse period and pulse amplitude are assumed to be independent, log normally distributed random variables. Their mutual independence is crucial for the validity of Equation 22. The rupture length is assumed to be uniformly distributed along the fault and the location of the hypocenter is assumed to uniformly distributed along the rupture length.

Numerical Implementation of the proposed PSDA analysis

Details on the numerical implementation of the proposed PSDA analyses are discussed in Sehhati (2008). Only a summary of important points is included herein for completeness. A schematic flow chart is presented in Figure 5. Note that the implementation was described for a single fault. For multiple faults, hazard is computed for each fault individually and then it is added to compute the overall hazard. All the probability distributions used in the implementation are bounded at ±3 standard deviations. The probability density functions are renormalized such that they satisfy all necessary conditions.

Equation 2 requires the definition of $d\lambda_{Sa}$. $d\lambda_{Sa}$ can be approximated by discretizing S_a into bins and taking $d\lambda_{Sa} = \lambda_{Sa,i} - \lambda_{Sa,i-1}$ where i is a summation counter for a discrete version of Equation 2. This approach, however, is not practical because it forces the use of identical bin sizes in the PSHA analysis and the PSDA analyses. Alternatively, each of the resulting hazard curves for S_a can be interpolated using a piece-wise polynomial (e.g. cubic spline interpolation) and the derivatives can be found analytically. Hence, Equation 2 can then be expressed as:

$$\lambda_{EDP}(x) = \sum_i P[EDP \geq x \,|\, Sa_i] \,|\, \lambda'_{Sa}(Sa = Sa_i)\Delta Sa_i \,| \quad (23)$$

Where $\lambda'_{Sa}(Sa=Sa_i)$ is the derivative of λ_{Sa} obtained analytical from the piece-wise polynomial interpolation of λ_{Sa} at Sa=Sa_i, and ΔSa_i is the bin size for Sa.

The heaviest computational cost of the proposed method lies in the definition of the response surface *EDP* (T_p, A_p). Note that because of the short duration of the equivalent pulses, the computational cost for defining the response surface is not nearly as significant as it would be for recorded ground motions. Moreover, structural reliability methods could be used to define the response surface in probabilistic terms (e.g. $P(EDP>x|T_p, A_p)$, in which case variations due to structural response (in addition to those due to input motion variability which are considered in this study) can be also included in the analyses.

Results

To illustrate the methodology presented in this work, a PSDA analysis is conducted for the 7-story structure previously described. The structure is located at various distances from an arbitrary fault. The structure is assumed to be on rock. In this example, only the fault normal component is considered, and it is assumed that the weak axis of the building is oriented in the fault normal direction. The Maximum Inter-story Ductility Demand (MIDD) is selected as the EDP for the analysis based on considerations discussed above.

Fault and Site Information

A 240 km vertical strike-slip fault was considered as the single seismic source. An arbitrary coordinate system as shown in the figure was assigned. A truncated exponential model was used to define the probability density function for magnitude. A seismicity rate of 1 was used for simplicity and a minimum magnitude of $M_w = 5.0$ was considered, assuming that lower magnitude earthquake do not contribute to hazard. Rupture lengths corresponding to each magnitude were estimated based on Wells and Coppersmith (1994):

$$\log(RLD) = -2.57 + 0.62M_w \quad \text{with} \quad \sigma = 0.15 \tag{26}$$

where *RLD* is the mean value of the rupture length and σ is the standard deviation in log units for the rupture length. The rupture length is assumed to follow a log normal distribution. The fault was assumed to be a linear source and its depth was neglected which assumes that the fault has a uniform probability of rupture along its depth and length. Shear velocity of the rock (V_s) was

assumed as 760 m/sec. Depth to V_S=1.0 km/s at the site (defined as Z_1 in Abrahamson and Silva NGA) was taken as 23.5 m.

Locations at various distances from the fault were considered in order to study the effect of forward-directivity based on source-site distance. For comparison purposes, PSDA analysis that do not include directivity and other analyses that include directivity with traditional approaches were also conducted, Hence, hazard for each location was calculated using four separate methodologies: A PSDA analysis that does not include forward directivity (henceforth called Traditional-PSDA); a PSDA model that includes forward directivity through the broadband model of Somerville et al. (1997), henceforth called Broadband-PSDA; the same model but modified such that the EDP for pulse scenarios is computed by Equation 4 (henceforth called Enhanced-Broadband-PSDA), and the proposed time-domain PSDA, henceforth called New-PSDA.

Results

The PSDA analyses were conducted for three points along the centerline of the fault and at varying distances from the fault (6 km, 11 km, and 21 km from the fault). Results are shown in Figure 6. As expected, the PSDA analysis that does not account for forward-directivity effects underestimates the hazard in near-fault zone compared to the other PSDA models. The maximum difference between hazard predicted from the aforementioned methods occurs for sites close to the fault and reduces as the distance from the fault increases or as the hazard level decreases (shorter return period). Results from PSDA analysis without directivity converge to those including directivity at distances from the fault greater than about 20 km.

Note that the inclusion of directivity using the proposed approach results, in general, in higher hazard than that obtained from the Broadband-PSDA model and the Enhanced-Broadband-PSDA, the latter being closer to the results of the proposed model. Recall that both the Enhanced-Broadband-PSDA and the New-PSDA models consider the special response of the structure to pulse-like motions, the Enhanced-Broadband-PSDA does it through separate relationships between EDP and $S_a(T_1)$ for pulse- and non-pulse-like ground motions, while the New-PSDA does it through time-domain analyses. Time domain analyses capture a more “fine-tuned” structural response and as a result predict higher hazard for nearly all scenarios.

In Figure 6, the contributions to hazard to the Enhanced-Broadband-PSDA model are divided into the hazard due to pulse motions (BB-Pulse) and hazard due to non-pulse motions (BB-No Pulse). Observe how at low return periods, the hazard is controlled by non-pulse motions while the reverse is true for long return periods. This occurs because the likelihood of occurrence of pulse-scenarios is very low hence at low return periods there is a minimal contribution to hazard by these scenarios. On the other hand, at long return periods, non-pulse scenarios cannot contribute significantly to hazard because of the low probability that such scenarios can generate large MIDDs. Similarly, the hazard predicted by the New-PSDA model is summation of near-source scenarios with dominant pulses (NS-P-in), near-source scenarios with pulses but where the pulse does not control the response of the structure (NS-P-out), near-source scenarios without pulses (NS-NP) and non near-source scenarios (Non-NS). As expected, the Non-NS scenario does not contribute to hazard for any of the distances considered. Similarly near-source pulse scenarios that are outside the range where the pulse is dominant contribute little to hazard. This is because these scenarios have a very low probability of occurring (for example, for a site at 11 km from the fault, the probability of a near-source scenario with pulses is only 0.4%, and of those only 0.21% are scenarios with pulses outside of the range where the pulse is dominant). At low return periods, most of the hazard results from non-pulse scenarios (which contribute nearly 99.5% of all possible scenarios), and the pulse scenarios that are in the range where pulses are dominant. Those scenarios, while constituting only (on average) 0.2% of all possible scenarios, contribute significantly to hazard because time-domain analyses do predict large EDPs for these scenarios.

Figure 7 shows the magnitude-distance deaggregation of hazard for some of the cases considered in Figure 6. Several interesting observations with significant relevance to hazard analysis can be inferred from the deaggregation plots. For close distances to the fault (Figure 6a), the proposed model predicts an increase in the contribution to hazard from small magnitude earthquakes. This difference is due to the ability of the time-domain analyses to capture the large EDPs that result from resonance when the pulse period matches the structural period. When forward-directivity is included through a broad-band model the effect of the pulse-type motions on the response spectra is smeared over a broad period band and the particular resonance that develops with pulse-type motions is not captured. For example, the contribution for a

Magnitude-Distance bin centered at 6 km (Figure 7a) increases from 4.1% to 10.3% when considering time domain analyses (the comparison is with the enhanced broadband model that considers pulse motions through $Sa(T_1)$). Equally important, the contribution of more distant earthquake increases significantly. For example, the time domain PSDA predicts a small contribution to hazard of low magnitude earthquakes for distances up to 15 km (up to 5% contribution to hazard), while the enhanced broadband model predicts no contribution to hazard for distances higher than 6 km. The same pattern (e.g. increase in the contribution to hazard of small earthquakes) persists even for distances of 21 km from the fault (Figure 7b) but is not present at larger distances.

Figure 8 plots the magnitude-distance deaggregation of the New-PSDA model separated into the contributions of near-source and far-source events, those with and without pulses, and those with pulses that control structural response. Magnitude and pulse-period deaggregation results show that as site-source distance increases, higher magnitudes contribute proportionally more to hazard. This is a results of a diminishing contribution of the pulse-controlled hazard (NS_P_in in Figure 8). Note that the contribution of near-source motions with dominant pulses (NS-P-in) dominates the contribution of small to intermediate magnitude earthquakes. This makes sense when one considers that a M_w 5.75 earthquake generates a pulse with a period of 1.1 sec, which is close to the period of the structure (1.0 sec). This confirms previous speculation that smaller magnitude earthquakes can contribute more to hazard than large magnitude earthquakes (Somerville 2003).

These observations have significant relevance for the design of structures in near-fault regions, as they indicate the importance of considering the near-source pulses for smaller magnitude earthquakes. For these cases, it is necessary to consider pulse-like motions in evaluating hazards. Hence, a deaggregation of pulse period and pulse amplitude can guide the selection of design ground motions. Figure 9 shows a deaggregation of pulse-period and pulse-amplitude for site-to-fault distances of 6 km and 21 km. This plot can be used directly to select simplified pulses that contribute the most to hazard. For example, it is obvious that pulse periods between 0.75 sec and 1.5 sec control design for a structure at 6 km from the fault, and the dominant pulse amplitude is centered around 30 cm/sec. Simplified pulses with these characteristics can be selected for the design of this particular structure. Observe that for larger

fault-to-site distances, the relative contribution of closer distances increases, but the dominant period remains centered around the period of the structure.

Figure 10 shows contours of the percentage difference in hazard predicted by a model without forward directivity and the broadband model that incorporates a separate measure for pulse-like motions (enhanced broadband model). Observe that the hazard increases by about 30% for regions close to the fault. this differences decreases to zero at about 25 km. In general, the hazard predicted by the proposed model is highest near the center and the edges of the fault. Figure 11 is similar to Figure 10, except that the hazard of the proposed model is compared to a model without forward directivity. In this case, the hazard increases by 60% for regions close to the fault. This increase diminishes to zero at a distance of about 25 km from the fault. This figures highlight the importance of considering forward directivity in hazard analysis, and the improvement in hazard characterization when the proposed model is used.

Conclusions and Recommendations

Hazard computations with the proposed methodology results in higher computed hazard for MIDD for the selected structures for sites located near to the fault. This increase results from the different treatment of pulse-like motions: whereas existing methodologies consider near-fault hazard through average increase in response spectral estimates, the proposed methodology captures its narrowband nature. Moreover, by performing structural analyses for each realization of the pulse-type motions, the resonant nature of the structural response to pulse-like motions is captured and introduced into the hazard computation.

Analysis with the proposed methodology indicated that near-source structures with structural periods close to about 1.0 seconds can be affected by smaller magnitude earthquakes that generate ground motion pulses with periods close to the structural period. Traditional, spectral acceleration-based PSDA analysis do not capture this effect and underestimate the contribution to hazard from small magnitude earthquakes and can lead to errors in ground motion selection for design.

Although the example selected in this report corresponds to an idealized MDOF structure and an idealized fault, both the fault model and the structural model were selected to represent realistic conditions and the results shown would very likely be reproduced for actual structures

located near active faults. Therefore, it is recommended that the proposed methodology be used for the design of transportation infrastructure located near faults, in particular for infrastructure whose failure can result in significant disturbance of road networks immediately after an earthquake. The proposed methodology not only computes a more adequate hazard from existing faults, but also provides, through pulse-period and pulse-amplitude disaggregation, a tool for selecting ground motions for design of such structures.

Recommendations for further study

Recommendations for further study are discussed below. Some of these recommendations were part of proposed tasks from the proposal presented to Transnow that resulted in the project whose results are presented in this work. These tasks were not included because the amount of time invested in the development of the proposed methodology had been underestimated.

- Some of the components of the model presented herein have not yet been fully developed. For example, the computation of near-fault hazard for non-pulse-type motions should be performed using a complete ground motion database that excludes non-pulse near-source motions. Such a task is beyond the scope of this research, yet it can be achieved thanks to the recent compilation of the NGA database. Another component that needs to be improved are the predictive models for PGV and pulse period. These models, understandably, are poorly constrained by existing data. Additional constraints from modeling or possibly with data collected from future earthquakes are necessary to generate more robust models.
- The model presented herein should be applied to actual transportation structures located near actual faults. Such a structural model has been previously developed at Washington State University (Bonvalot 2006) for two bridges located near the Seattle fault, and was enhanced through the work performed in this project. A characterization of the Seattle fault is summarized by Gillie (2006). This task had originally been proposed for this research but time constrained prevented its realization.
- The proposed model can be easily applied to geotechnical structures such as retaining walls or man-made slopes. Such structures can also be affected by the same resonance phenomenon that leads to high structural response to pulse-like ground motions. This

task had originally been proposed for this research but time constrained prevented its realization.

- The analyses presented herein assumed that the structure is has a weak axis aligned with the fault normal direction. While theory predicts that forward-directivity pulses are aligned with the fault normal direction, actual recordings indicated that the orientation of these pulses is a random variable. This variability should be considered when making estimates of hazard to structures.

REFERENCES

Abrahamson, N., and Silva, W. (2007). "NGA Ground Motion Relations for the Geometric Mean Horizontal Component of Peak and Spectral Ground Motion Parameters." Pacific Earthquake Engineering Research Center College of Engineering, University of California, Berkeley.

Abrahamson, N.A. (2000). "Effects of rupture directivity on probabilistic seismic hazard analysis", Proceedings of the Sixth International Conference on Seismic Zonation, Earthquake Engineering Research Inst., Oakland, California.

Alavi, B., and Krawinkler, H. (2000) "Consideration of near-fault ground motion effects in seismic design." Proceedings, 12th World Conference on Earthquake Engineering, New Zealand, 1-8.

Anderson, J. C., and Bertero, V. V. (1987). "Uncertainties in establishing design earthquakes." ASCE Journal of Structural Engineering, 113(8), 1709-1724.

ATC-58. (2004). "Engineering Demand Parameters for Structural framing System." Project Task Report, Applied Technology Council, Redwood City, CA.

Baker, J. (2007). "Quantitative classification of near-fault ground motions using wavelet analysis." Bulletin of the Seismological Society of America, 97(5), 1486-1501.

Bonvalot, E. (2006). “Dynamic response of bridges to near-fault, forward directivity ground motions.” M.S. Thesis, Washington State University, Pullman, WA.

Bray, J. D., and Rodriguez-Marek, A. (2004). "Characterization of forward-directivity ground motions in the near-fault region." Soil Dynamics and Earthquake Engineering, 24, 815-828.

Chopra, A. (1995). Dynamics of structures, Prentice Hall, Englewood Cliffs, NJ.

Chopra, A. K., and Chintanapakdee, C. (2001). "Comparing response of SDF systems to near-fault and far-fault earthquake motions in the context of spectral regions." Earthquake engineering and Structural Dynamics, 30, 1769-1789.

Cornell, C. A., Jalayer, F., Hamburger, R. O., and Foutch, D. A. (2002). "Probabilistic basis for 2000 SAC Federal Emergency Management Agency steel moment frame guidelines." Journal of Structural Engineering, 128(4), 526-533.

Gabor, D. (1946). "Theory of communication." IEEE, 93, 429-41.

Gillie J.L. (2005). Nonlinear Response Spectra of Forward-Directivity Ground Motions. MSc Thesis, Washington State University, Pullman, WA.

Hall, J. F., Heaton, T. H., Halling, M. W., and Wald, D. J. (1995). "Near-source ground motion and its effects on flexible buildings." Earthquake Spectra, 11(4), 569-605.

Iervolino, I., Cornell, C.A. (2008). Conditional Pulse Probability for Near-Source Hazard Analysis, the 14th World Conference on Earthquake Engineering, October 12-17, 2008, Beijing, China.

Makris, N. (1997). "Rigidity-plasticity-viscosity: can electro rheological dampers protect base-isolated structures from near-source ground motions." Earthquake Engineering Structural Dynamics, 26, 571–91.

Malhotra, P. K. (1999). "Response of Buildings to Near-Field Pulse-Like Ground Motions." Earthquake Engineering and Structural Dynamics, 28, 1309-1326.

Mavroeidis, G. P., and Papageorgiou, A. S. (2003). "A mathematical representation of near-fault ground motions." Bulletin of the Seismological Society of America, 93(3), 1099-1131.

McGuire, R. K. (2004). Seismic hazard and risk Analysis, Earthquake Engineering Research Institute, Boulder, Colorado.

Mylonakis, G., and Reinhorn, A. (2001). "Yielding oscillator under triangular ground acceleration pulse." Journal of Earthquake Engineering, 5, 225-51.

PEER. (1999). "Pacific Earthquake Engineering Research Center, strong motion database. http://peer.berkeley.edu/smcat/search.html."

Priestley, M. J. N. (2003). Myths and fallacies in earthquake engineering, revisited: The Malley-Milne lecture. Rose School, Collegio Allessandro Volta, Pavia, Italy.

Sasani, M., and Bertero, V. V. "Importance of severe pulse-type ground motions in performance-based engineering: historical and critical review." Proceedings, 12th World Conference on Earthquake Engineering, New Zealand, 1-7.

Sehhati, R. (2008). “Probabilistic seismic demand analysis for the near-fault zone.” Ph.D. Dissertation, Washington State University, Pullman, WA.

Somerville, P. G. (2003). "Magnitude scaling of the near fault rupture directivity pulse." Physics of the Earth and Planetary Interiors, 137, 201-212.

Somerville, P. G., Smith, N. F., Graves, R., and Abrahamson, N. A. (1997). "Modification of Empirical Strong Ground Motion Attenuation Relations to Include the Amplitude and Duration Effects of Rupture Directivity." Seismological Research Letters, 68(1), 199-222.

Spudich, P., and Chiou, B. (2008). "Directivity in NGA earthquake ground motions: analysis using isochrone theory." Earthquake Spectra, 24(1), 279-98.

The MathWorks Inc. "MATLAB Version 7.1.0.246, Revision 14, Service Pack 3, ©1984-2005. http://www.mathworks.com/."

Tothong, P., Cornell, C.A., Baker, J.W., 2007, Explicit Directivity-Pulse Inclusion in Probabilistic Seismic Hazard Analysis, Earthquake Spectra, Volume 23, No. 4, pages 867–891, Earthquake Engineering Research Institute.

Wells, D.L., Coppersmith, K.J. (1994), New Empirical Relationship Among Magnitude, Rupture Length, Rupture Width, Rupture Area, and Surface Displacement, BSSA, Vol. 84, No. 4, pp. 974-1002.

Zhang, Y., and Iwan, W. (2002). "Active interaction control of tall buildings subjected to near-field ground motions." Journal of Structural Engineering, 128, 69-79.

Figures

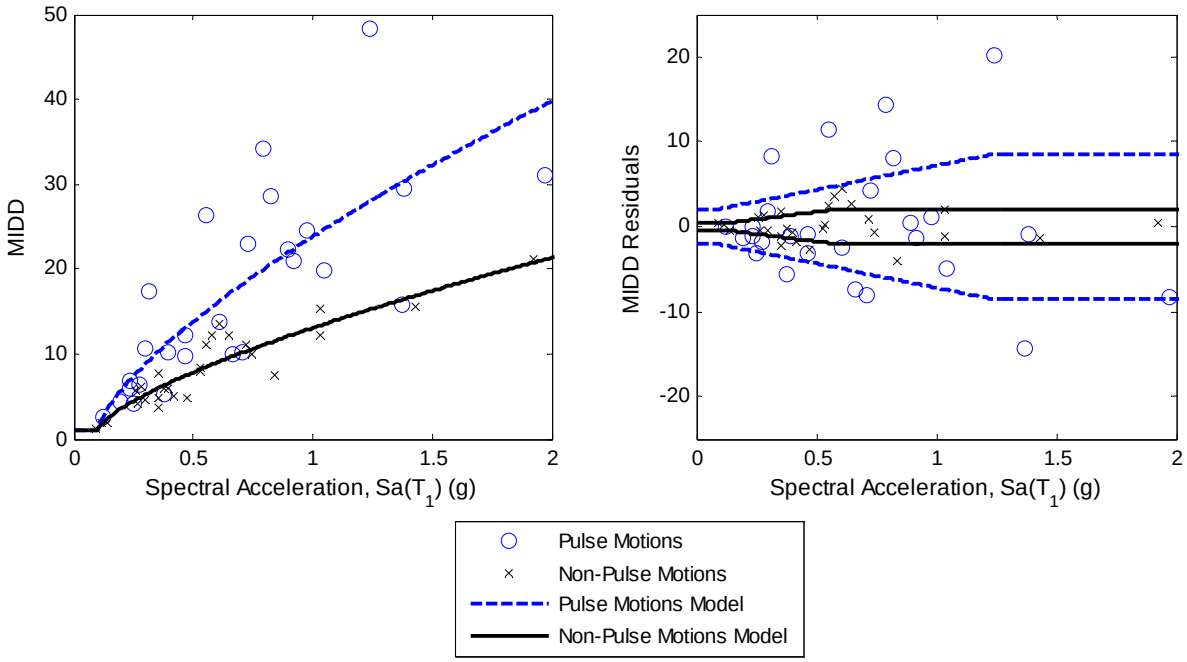

Figure 1. Predictive model for Maximum Interstory Ductility Demand (MIDD) as a function of spectral acceleration at the first mode period of the structure. On the left is the mode (Equations 3 and 4). On the right, the residuals (MIDD for each record minus the predictive MIDD for the Sa(T1) of each record) and the model for standard deviation (Equation 3b).

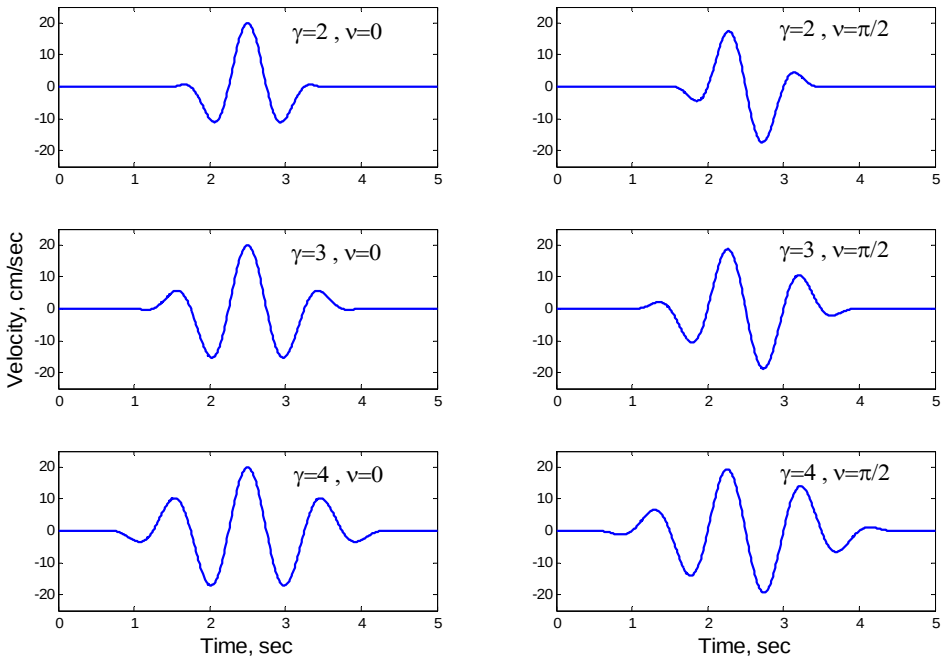

Figure 2: Gabor wavelet pulses with parameters A = 20 cm/sec, f_p = 1 Hz, and t_o = 2.5 sec.

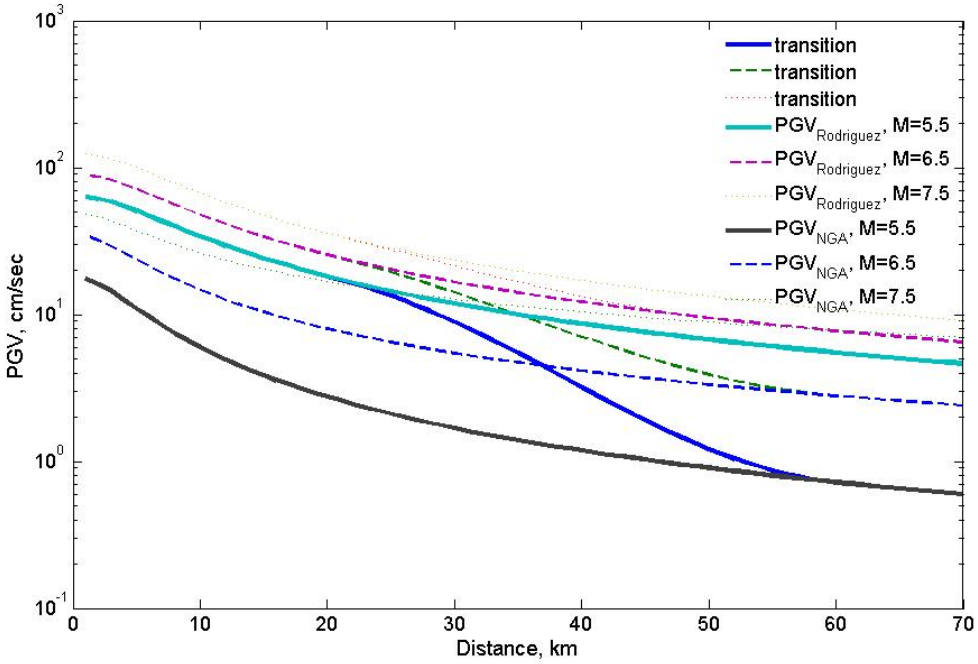

Figure 3: Transition from PGV estimated by Bray and Rodriguez-Marek (2004) to PGV estimated by Abrahamson and Silva (2007) for distances between 20 and 60 km.

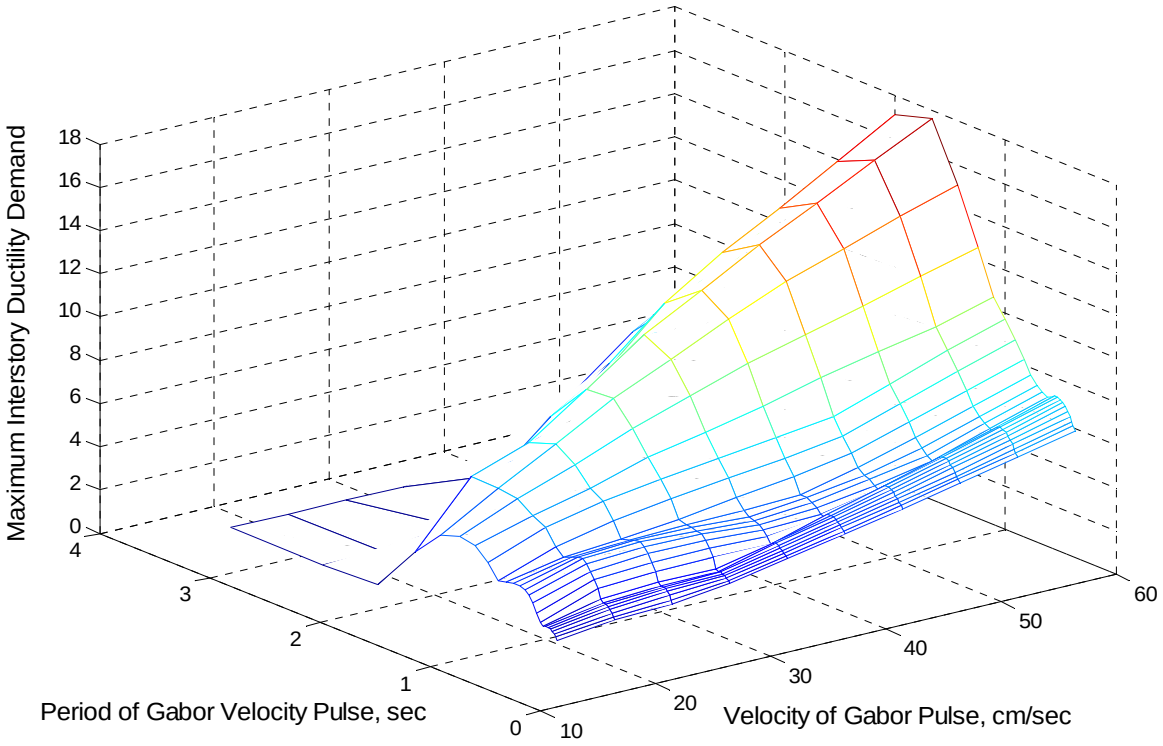

Figure 4: Maximum inter-story ductility demand of the 7-story structure for Gabor pulses with parameters $\gamma = 3$, $15 < A < 60$ cm/s, and $0.37 < T_p < 3.33$ s.

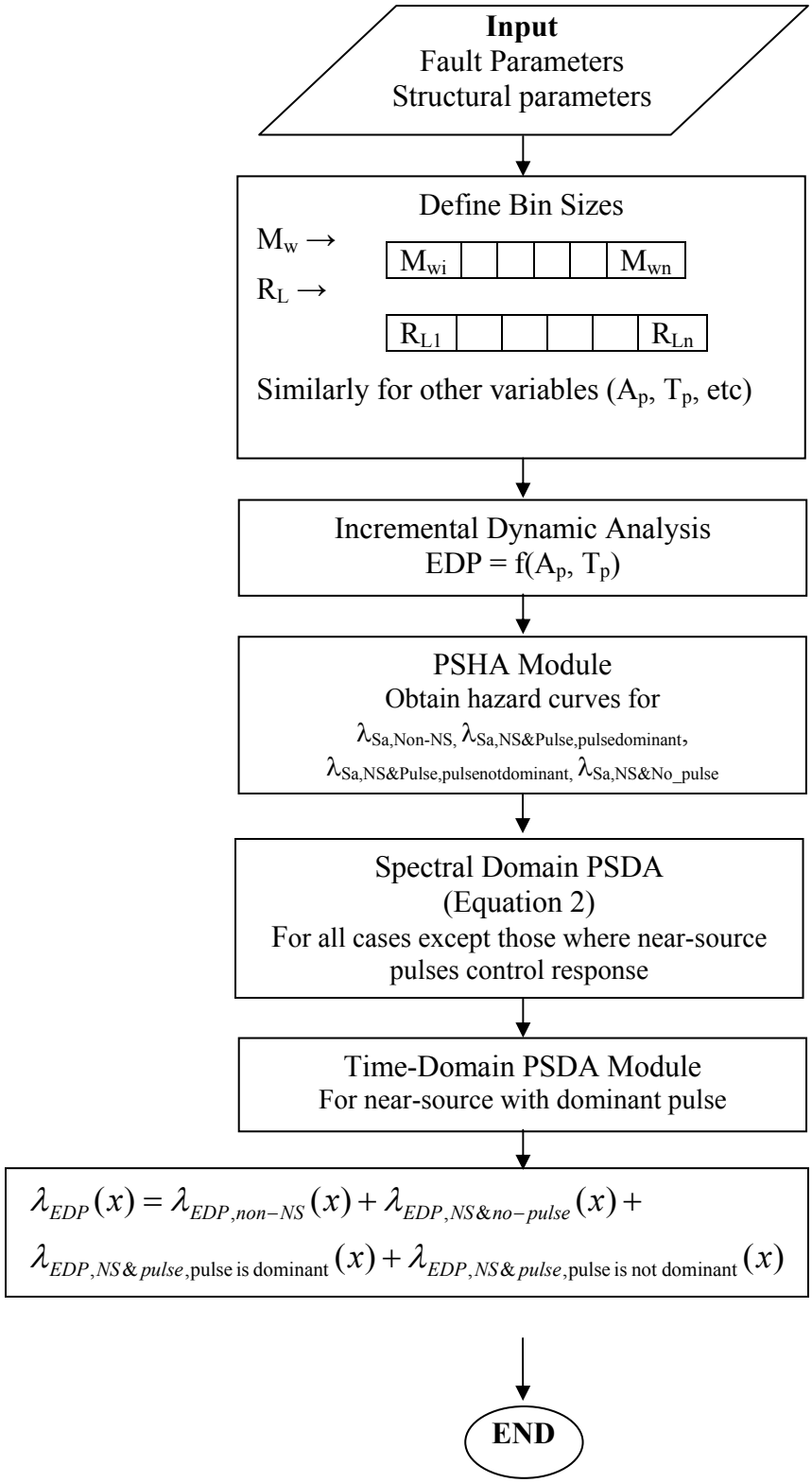

Figure 5. Implementation flow chart. For details see Sehhati (2008).

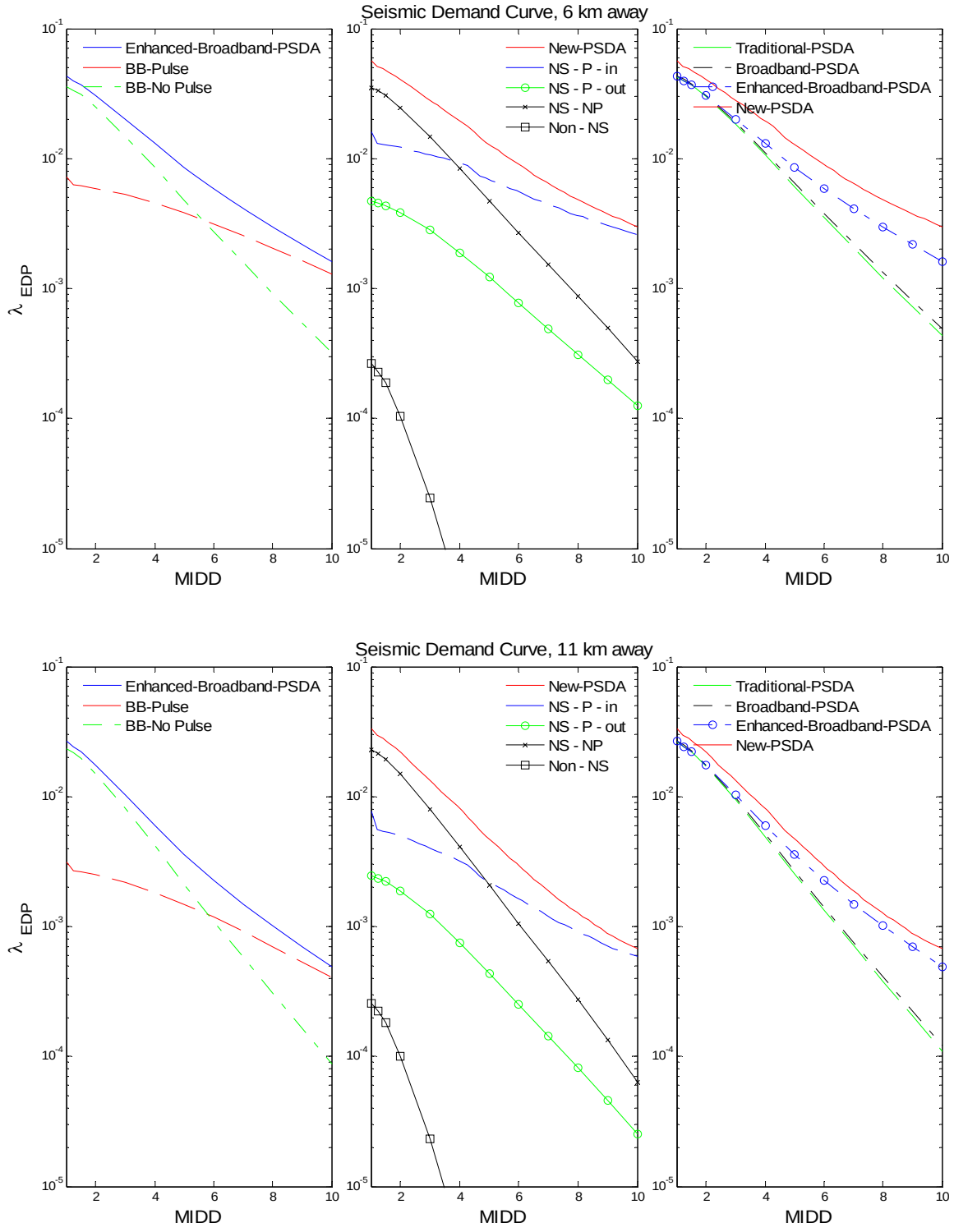

Figure 6a. Mean annual frequency of exceedance of EDP (λ_{EDP}) for sites located along the centerline of the fault at 6 and 11 km from the fault.

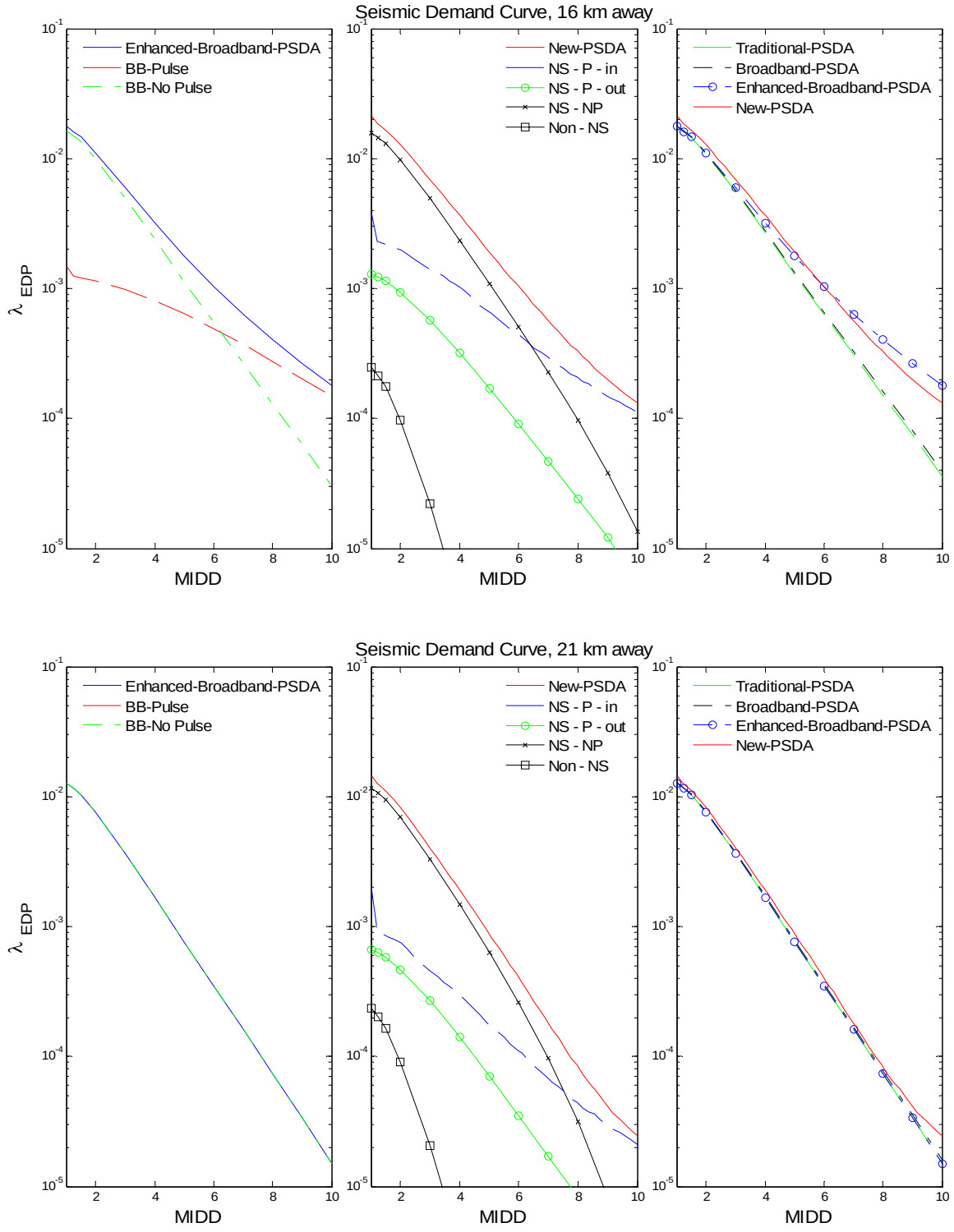

Figure 6b. Mean annual frequency of exceedance of EDP (λ_{EDP}) for sites located along the centerline of the fault at 16 and 21 km from the fault.

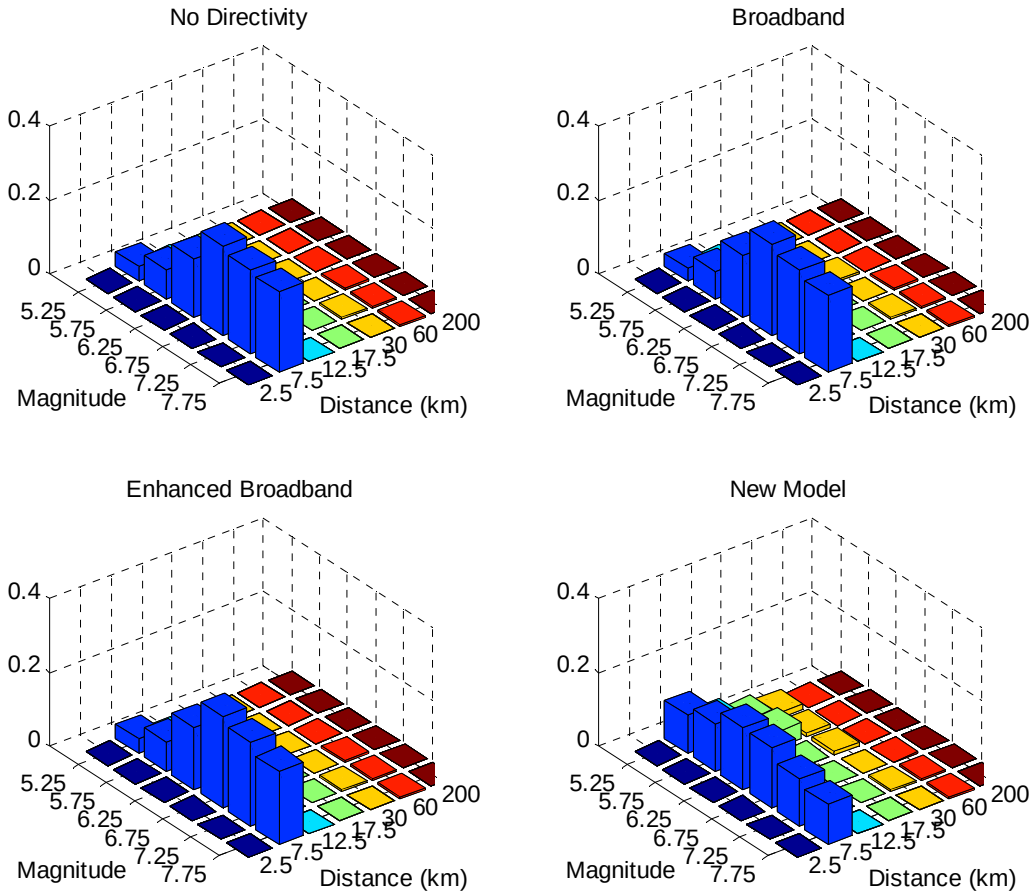

Figure 7a. Magnitude-Distance deaggregation for EDP > 5 and for a site along the centerline of the fault at 6 km from the fault. The y-axes correspond to the percentage contribution to hazard for each of the four different analyses.

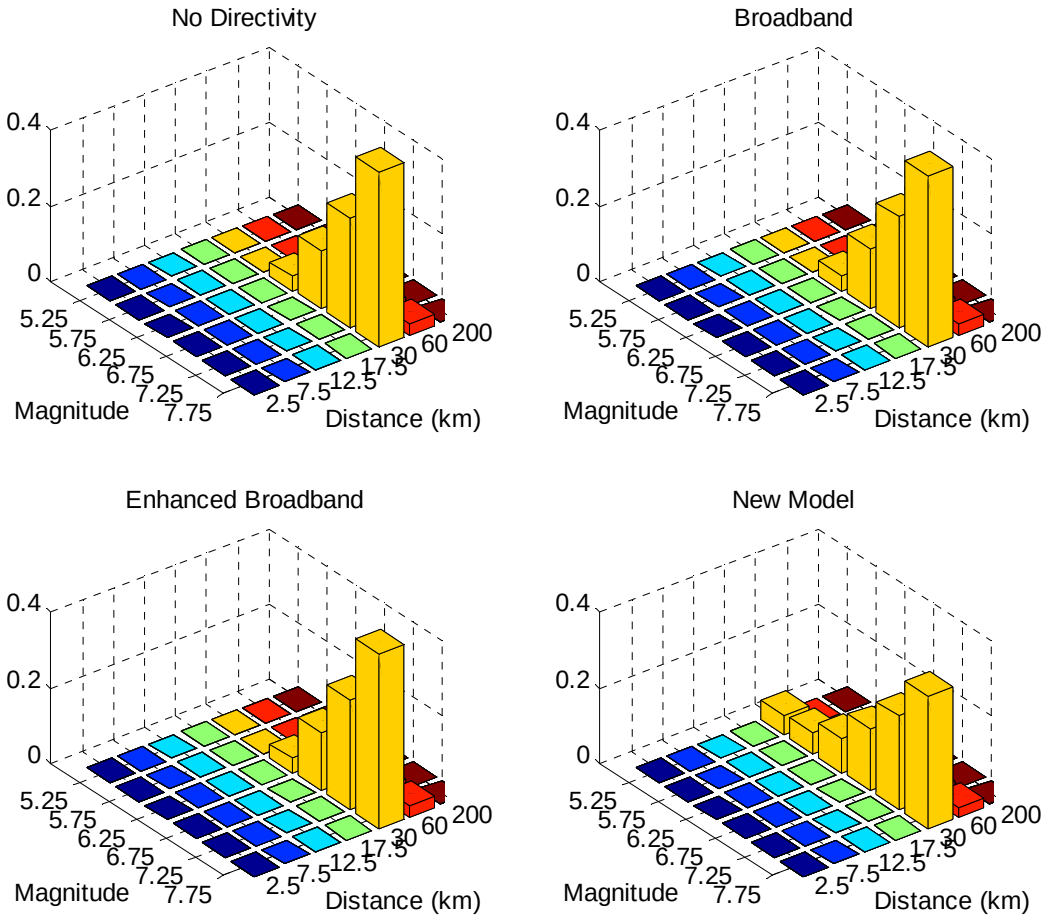

Figure 7b. Magnitude-Distance deaggregation for EDP > 5 and for a site along the centerline of the fault at 21 km from the fault. The y-axes correspond to the percentage contribution to hazard for each of the four different analyses.

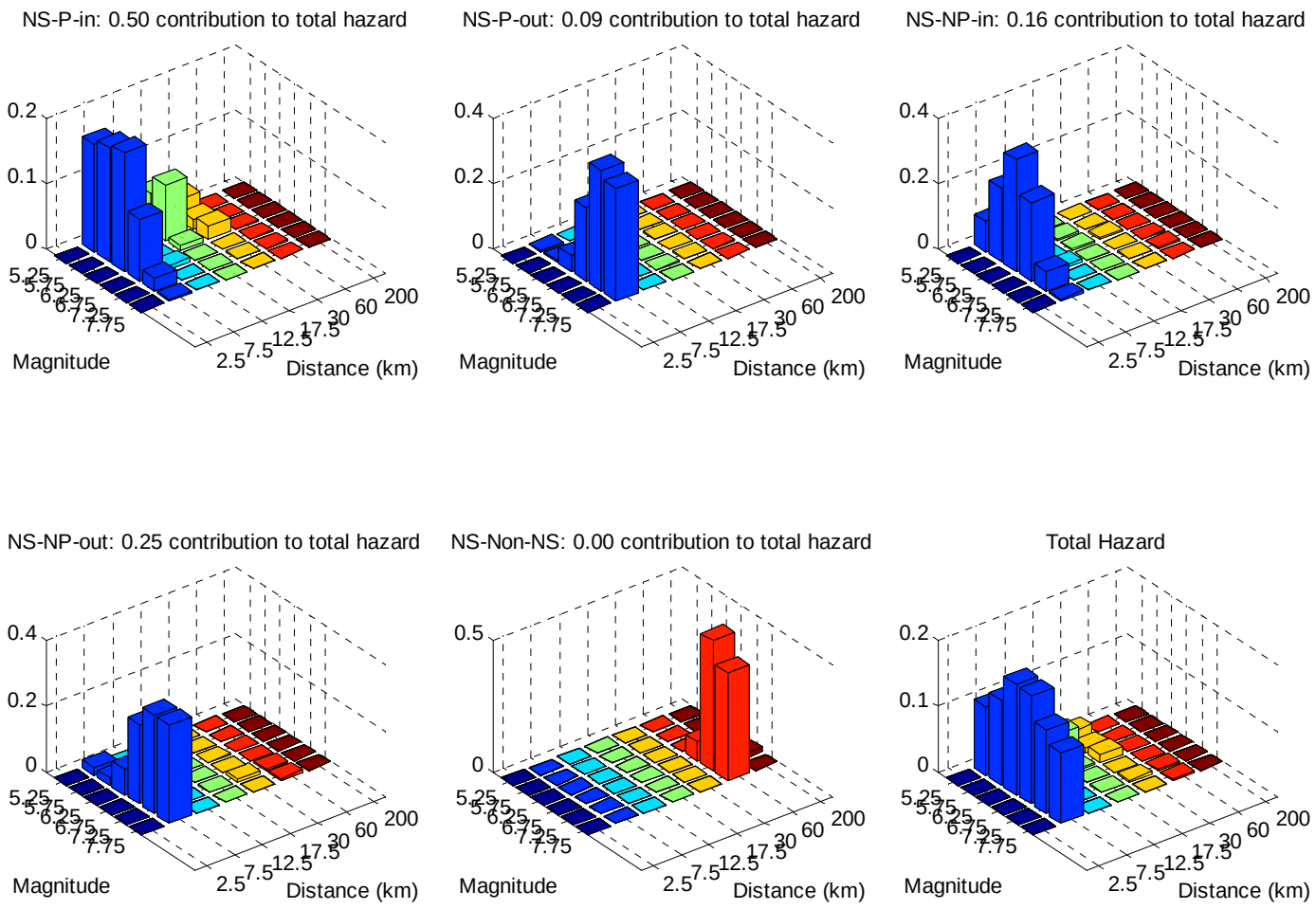

Figure 8a. Magnitude-Distance deaggregation for EDP > 5 and for a site along the centerline of the fault at 6 km from the fault. Different deaggregations are shown for different components of hazard of the proposed PSDA model. The title of each figure indicates the percentage contribution total hazard.

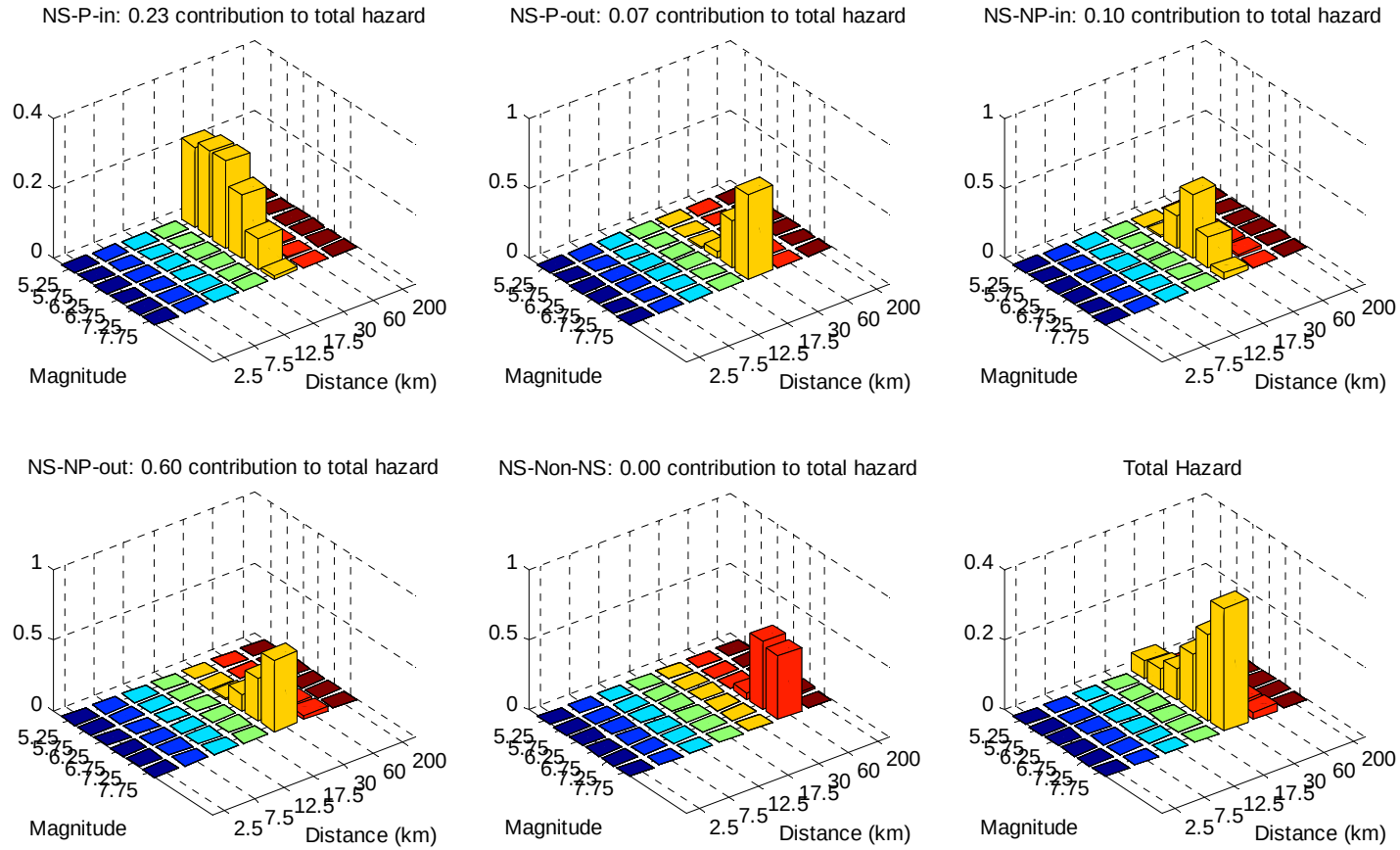

Figure 8b. Magnitude-Distance deaggregation for EDP > 5 and for a site along the centerline of the fault at 21 km from the fault. Different deaggregations are shown for different components of hazard of the proposed PSDA model. The title of each figure indicates the percentage contribution total hazard.

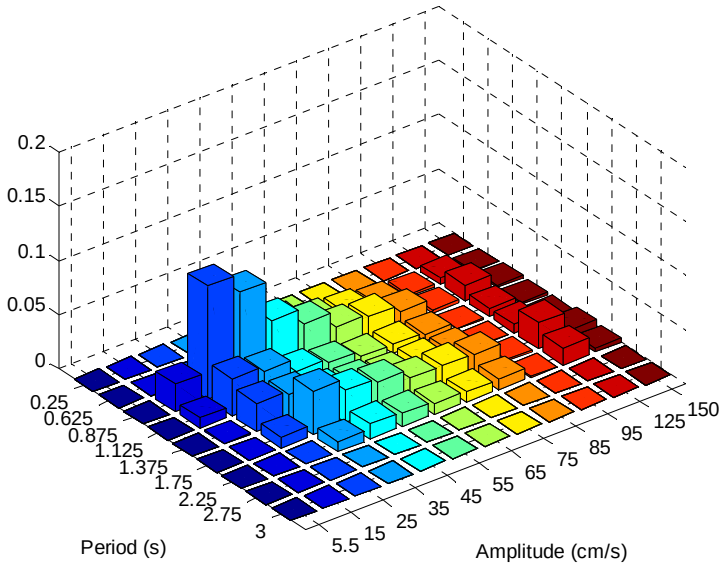

a)

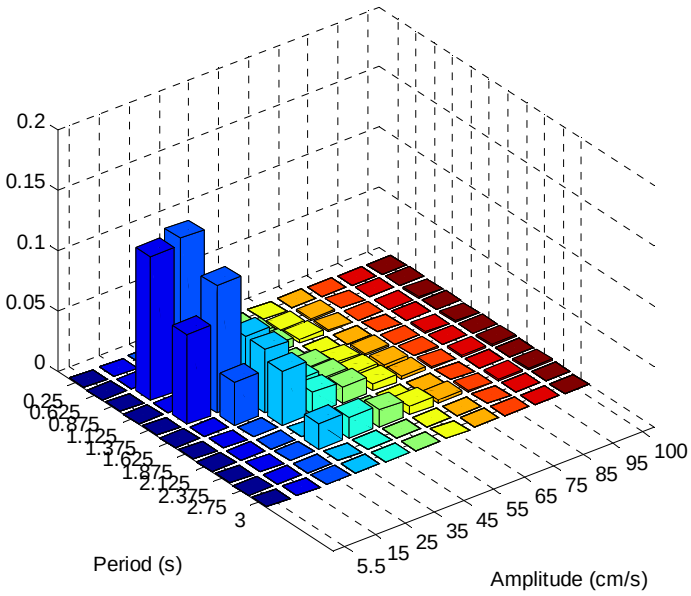

b)

Figure 9. Pulse period and pulse amplitude deaggregation for two sites along the centerline of the fault: a) at 6 km and b) at 21 km from the fault. The y axis shows the percentage contribution

to hazard only with respect to pulse-like scenarios where the pulse is dominant. These scenarios contribute 50% and 23% of total hazard for distances of 6km and 21 km, respectively.

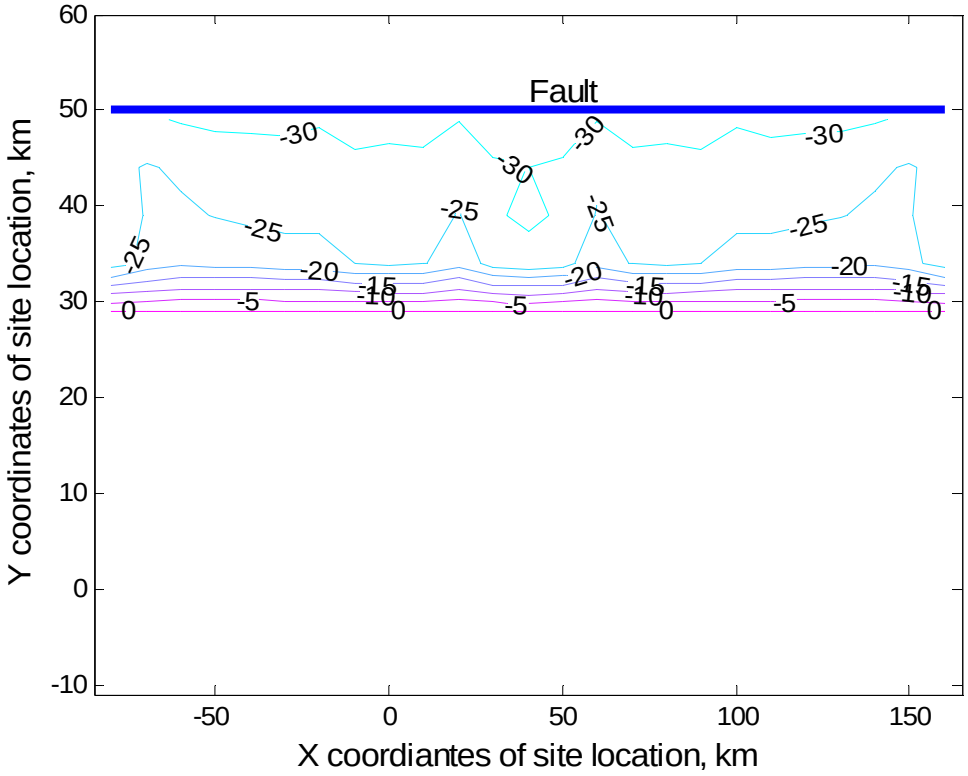

Figure 10: Contours variations of λ_{EDP} for EDP > 5 predicted by PSDA without forward directivity and the Enhanced-Broadband-PSDA. Observe that maximum increase of hazard occurs near the center and the edges of the fault.

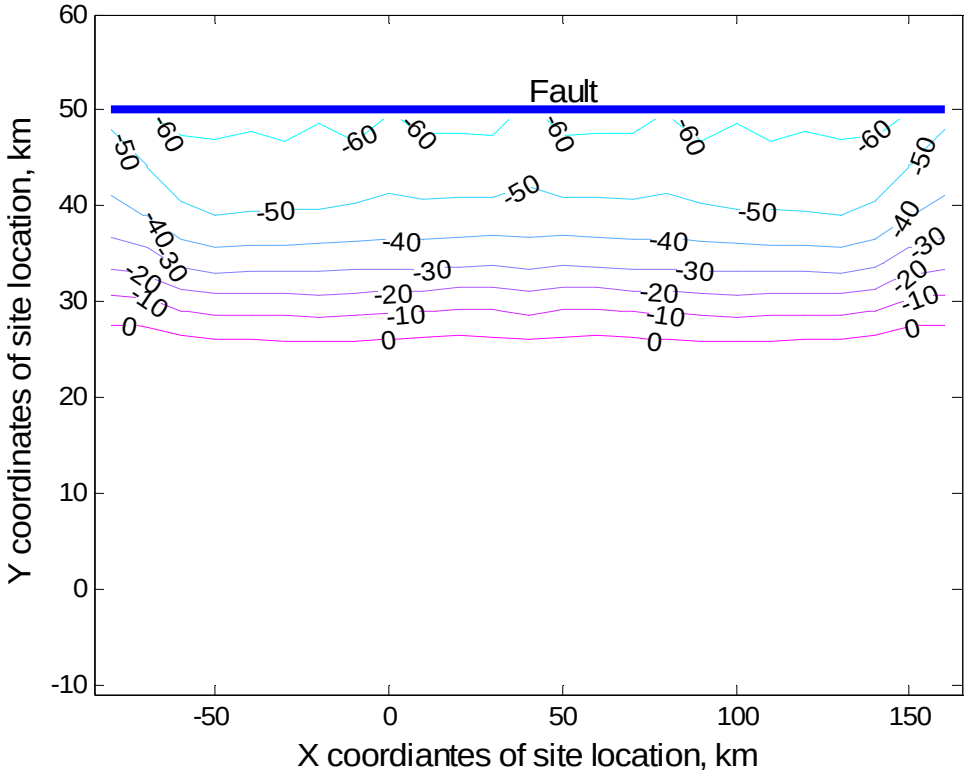

Figure 11. Contours variations of λ_{EDP} for EDP > 5 predicted by PSDA without forward directivity and the proposed PSDA analysis.

Appendix A

Ground motions used in this study

Table A1: Earthquakes that recorded the ground motions used in this study.

Earthquake	Date	Moment magnitude
Parkfield (PF)	6/27/66	6.1
San Fernando (SF)	2/9/71	6.6
Imperial valley (IV)	10/15/79	6.5
Morgan Hill (MH)	4/24/84	6.2
Superstition Hills (SH)	11/24/87	6.6
Loma Prieta (LP)	10/17/89	7
Erzincan, Turkey (EZ)	3/13/92	6.7
Landers (L)	6/28/92	7.3
Northridge (N)	1/17/94	6.7
Kobe (KB)	1/17/95	6.9
Kocaeli (K)	8/17/99	7.4
Chi-Chi (CH)	9/21/99	7.6
Duzce (D)	11/12/99	7.1
Palm Springs (PS)	7/8/86	6.0
Denali(DE)	11/3/02	7.9
San Simeon (SS)	12/23/03	6.5
Bam (B)	12/26/03	6.5

Table A2: Ground motions with forward-directivity effects (selected from Bray and Rodriguez-Marek (2004)).

#	Station	Agency	Station #	Event[a]	R[b] (km)	Site[c]	PGA (g)	PGV (cm/s)	$T_{v\text{-}p}$ [e](s)	$(T_p)_{Baker}$ [f] (s)	$(A_p)_{Baker}$ [g] (cm/s)
1	Gilroy-Gavilan Coll.	CDMG	47006	LP	11.6	r	0.32	30.81	0.38	1.80	13.8
2	Gilroy-Historic Bldg.	CDMG	57476	LP	12.7	s	0.29	36.82	1.47	1.80	29.2
3	Gilroy Array#1	CDMG	47379	LP	11.2	r	0.48	38.61	0.4	4.31	9.4
4	Gilroy Array#2	CDMG	47380	LP	12.7	s	0.41	45.67	1.46	1.72	40.4
5	Gilroy Array#3	CDMG	47381	LP	14.4	s	0.54	49.34	0.48	2.32	23.8
6	LGPC	UCSC	16	LP	6.1	r	0.84	103.18	0.79	3.92	62.1
7	Saratoga-Aloha Ave.	CDMG	58065	LP	13.0	s	0.39	55.58	1.55	4.47	26.5
8	Saratoga-W Valley Coll.	CDMG	58235	LP	13.7	s	0.40	71.33	1.14	1.90	37.7
9	Erzincan		95	EZ	2.0	s	0.50	95.56	2.23	2.65	66.6
10	Jensen Filtration Plant	USGS	655	N	6.2	s	0.40	104.55	2.86	3.36	80.3
11	Newhall-Fire Sta.	CDMG	24279	N	7.1	s	0.77	120.27	0.71	1.04	92.6
12	Newhall-W. Pico Can. Rd	USC	90056	N	7.1	s	0.43	87.75	2.03	2.41	76.0
27	Pacoima Dam (downstr.)	CDMG	24207	N	8.0	r	0.53	51.24	0.44	0.59	35.0
14	Rinaldi Receiving Sta.	DWP	77	N	7.1	s	0.89	173.07	1.06	1.50	111.3
15	Sylmar-Converter Sta.	DWP	74	N	6.2	s	0.61	130.27	1.1	3.48	78.4

Table (Cont.)

#	Station	Agency	Station #	Event[a]	R[b] (km)	Site[c]	PGA (g)	PGV (cm/s)	$T_{v\text{-}p}$ [e] (s)	$(T_p)_{Baker}$ [f] (s)	$(A_p)_{Baker}$ [g] (cm/s)
16	Sylmar-Converter Sta. E.	DWP	75	N	6.1	s	0.85	116.56	2.92	3.49	55.0
17	Sylmar-Olive View FF	CDMG	24514	N	6.4	s	0.77	122.72	2.42	3.11	71.0
18	Pacoima Kagel Canyon	CDMG	24088	N	7.3	r	0.53	56.00	0.88	0.90	43.0
19	Arleta-Nordhoff Fire Sta.	CDMG	24087	N	8.7	s	0.32	35.50	1.49	1.23	23.0
13	Duzce	ERD	–	K	12.7	s	0.36	46.41	1.37	1.36	46.7
20	Arcelik Kandilli		–	K	17.0	r	0.14	42.35	5.24	7.97	28.4
21	Gebze	ERD	–	K	17.0	r	0.28	40.69	4.62	5.97	34.0
22	TCU052[h, i]	CWB	–	CH	0.2	s	0.53	177.27	4.48	6.12	95.2
23	TCU068[h]	CWB	–	CH	1.1	s	0.61	145.13	4.06	4.25	104.9
24	TCU075[i]	CWB	–	CH	1.5	s	0.32	76.14	2.03	2.41	61.8
25	TCU101[i]	CWB	–	CH	2.9	s	0.21	65.19	8.62	6.86	38.4
26	TCU102[i]	CWB	–	CH	1.8	s	0.30	87.07	2.52	9.11	51.7

[a] See Table .
[b] Closest distance to the fault plane.
[c] Soil (s) or rock (r).
[e] Period corresponding to the peak in the velocity response spectrum.
[f] Pulse period determined with the procedure of Baker (2007).
[g] Pulse amplitude determined with the procedure of Baker (2007).
[h] The fault normal direction for these records was assumed to be the direction oriented with the largest velocity pulse (N122º for TCU052 and N199º for TCU068).
[i] The fling step was removed using the procedure described in Bray and Rodriquez-Marek (2004).

TableA3 Near-fault ground motions included in the non-FD database (e.g. those that do not have pulse-like characteristics).

#	Station	Agency	Station #	Event[a]	R [b] (km)	Site[c]	PGA (g)	PGV (cm/sec)	T_{v-p} [d]
1	BRAN	UCSC	13	LP	10.7	r	0.63	53.34	0.49
2	Capitola	CDMG	47125	LP	15.2	s	0.45	34.56	0.64
3	Corralitos	CDMG	57007	LP	3.9	r	0.51	45.48	0.75
4	UCSC Lick Observatory	CDMG	15	LP	18.4	r	0.47	17.69	0.36
5	UCSC	UCSC	58135	LP	18.5	r	0.46	11.61	0.16
6	WAHO	UCSC	14	LP	17.5	r	0.78	25.42	0.23
7	N Hollywood – Coldwater Can.	USC	90009	N	12.5	r	0.24	22.89	1.2
8	Sunland – Mt Gleason Ave.	USC	90058	N	13.4	r	0.15	19.25	1.04
9	Burbank – Howard Rd.		90059	N	16.9	r	0.12	8.14	0.64
10	Simi Valley – Katherine Rd.	USC	90055	N	13.4	r	1.07	51.4	0.62
11	Sun Valley – Roscoe Blvd.	USC	90006	N	10.1	s	0.31	25.86	1.01
12	Santa Susana Ground	USGS	5108	N	16.7	r	0.4	20.31	0.69
13	Big Tujunga, Angeles Nat F	USC	90061	N	19.7	r	0.17	6.67	0.64
14	CHY028	CWB	-	CH	3.1	s	0.65	72.86	0.62
15	CHY029	CWB	-	CH	11.0	s	0.3	30.35	0.67
16	CHY035	CWB	-	CH	12.7	s	0.25	45.61	1.28
17	CHY080	CWB	-	CH	2.7	s	0.97	107.61	0.88
18	CHY006	CWB	-	CH	9.8	s	0.36	55.44	1.81
19	TCU055	CWB	-	CH	6.4	s	0.24	26.23	2.15
20	TCU070	CWB	-	CH	19.0	s	0.26	52.16	5.1
21	TCU071	CWB	-	CH	5.3	s	0.58	44.52	0.56
22	TCU072	CWB	-	CH	7.0	s	0.53	71.8	0.88
23	TCU074	CWB	-	CH	13.5	s	0.64	73.4	1.47
24	TCU079	CWB	-	CH	11.0	s	0.76	61.24	0.6
25	TCU089	CWB	-	CH	8.9	s	0.34	30.93	5.42

#	Station	Agency	Station #	Event[a]	R [b] (km)	Site[c]	PGA (g)	PGV (cm/sec)	T_{v-p} [d]
26	Bolu	ERD	-	D	17.6	s	0.81	56.51	0.79
27	Duzce	ERD	-	D	8.2	s	0.36	59.99	5.50

[a] See Table .

[b] Closest distance to the fault plane.

[c] Soil (s) or rock (r).

[d] Period corresponding to the peak in the velocity response spectrum.